frontiers in Immunology

ORIGINAL RESEARCH
published: 28 January 2019
doi: 10.3389/fimmu.2019.00004

Immunobiochemical Reconstruction of Influenza Lung Infection—Melanoma Skin Cancer Interactions

Evgeni V. Nikolaev[1,2], *Andrew Zloza*[3,4] *and Eduardo D. Sontag*[5,6,7]*

[1] Center for Quantitative Biology, Rutgers University, Piscataway, NJ, United States, [2] Clinical Investigations and Precision Therapeutics Program, Rutgers Cancer Institute of New Jersey, New Brunswick, NJ, United States, [3] Section of Surgical Oncology Research, Division of Surgical Oncology, Rutgers Cancer Institute of New Jersey, New Brunswick, NJ, United States, [4] Department of Surgery, Rutgers Robert Wood Johnson Medical School, New Brunswick, NJ, United States, [5] Department of Electrical and Computer Engineering, Northeastern University, Boston, MA, United States, [6] Department of Bioengineering, Northeastern University, Boston, MA, United States, [7] Laboratory for Systems Pharmacology, Harvard Medical School, Boston, MA, United States

It was recently reported that acute influenza infection of the lung promoted distal melanoma growth in the dermis of mice. Melanoma-specific CD8+ T cells were shunted to the lung in the presence of the infection, where they expressed high levels of inflammation-induced cell-activation blocker PD-1, and became incapable of migrating back to the tumor site. At the same time, co-infection virus-specific CD8+ T cells remained functional while the infection was cleared. It was also unexpectedly found that PD-1 blockade immunotherapy reversed this effect. Here, we proceed to ground the experimental observations in a mechanistic immunobiochemical model that incorporates T cell pathways that control PD-1 expression. A core component of our model is a kinetic motif, which we call a PD-1 Double Incoherent Feed-Forward Loop (DIFFL), and which reflects known interactions between IRF4, Blimp-1, and Bcl-6. The different activity levels of the PD-1 DIFFL components, as a function of the cognate antigen levels and the given inflammation context, manifest themselves in phenotypically distinct outcomes. Collectively, the model allowed us to put forward a few working hypotheses as follows: (i) the melanoma-specific CD8+ T cells re-circulating with the blood flow enter the lung where they express high levels of inflammation-induced cell-activation blocker PD-1 in the presence of infection; (ii) when PD-1 receptors interact with abundant PD-L1, constitutively expressed in the lung, T cells loose motility; (iii) at the same time, virus-specific cells adapt to strong stimulation by their cognate antigen by lowering the transiently-elevated expression of PD-1, remaining functional and mobile in the inflamed lung, while the infection is cleared. The role that T cell receptor (TCR) activation and feedback loops play in the underlying processes are also highlighted and discussed. We hope that the results reported in our study could potentially contribute to the advancement of immunological approaches to cancer treatment and, as well, to a better understanding of a broader complexity of fundamental interactions between pathogens and tumors.

Keywords: influenza, melanoma, PD-1/PD-L1, incoherent feedforward loop, mathematical modeling

OPEN ACCESS

Edited by:
Gennady Bocharov, Institute of Numerical Mathematics (RAS), Russia

Reviewed by:
Zvi Gershon Grossman, National Institute of Allergy and Infectious Diseases (NIAID), United States
Kirill Peskov, Modeling and Simulation Decisions, Russia

***Correspondence:**
Eduardo D. Sontag
e.sontag@northeastern.edu

Specialty section:
This article was submitted to Viral Immunology, a section of the journal Frontiers in Immunology

Received: *29 May 2018*
Accepted: *02 January 2019*
Published: *28 January 2019*

Citation:
Nikolaev EV, Zloza A and Sontag ED (2019) Immunobiochemical Reconstruction of Influenza Lung Infection—Melanoma Skin Cancer Interactions. Front. Immunol. 10:4. doi: 10.3389/fimmu.2019.00004

1. INTRODUCTION

It was recently reported that acute influenza A infection (A/H1N1/PR8) of the lung promoted distal B16-F10 skin melanoma growth in the dermis (1). It was also observed that melanoma-specific CD8+ T cells were shunted to the lung in the presence of the infection, where they expressed high levels of inflammation-induced cell-activation blocker PD-1, and became incapable of migrating back to the tumor site. At the same time, co-infection virus-specific CD8+ T cells remained functional while the infection was cleared. Finally, it was also unexpectedly found that blockade of PD-1 resulted in reversal of infection-mediated anti-tumor response disruption.

In this respect, it is very important to mention that the work by Kohlhapp et al. (1) was primarily motivated by two still unmet challenges: (i) emerging epidemiological studies reporting an increased cancer prevalence and cancer-specific deaths in patients with infections (1), and (ii) despite the fact that tremendous amount of work on immune response in the context of pathogenic co-infection has been done, findings in this field still remain discordant and a matter of debate, as also reviewed by Kohlhapp et al. (1) and Zloza (2).

Motivated by the need to provide a more conceptual and quantitative biology insight into "the previously unrecognized acute non-oncogenic infection factor" accelerating tumor growth (1) and more broadly into the interactions between pathogens and cancer, and specifically, in order "to harness these interactions to improve microbial-based cancer therapy" (2), we suggest a few immunobiochemical mechanisms and a simple mathematical model which may help to interpret the observed phenomena (1).

Our main results relate to two fundamental functional roles of immunity (3–5): (i) adaptation of immune function, and (ii) competition between excitation and de-excitation ("push-pull") factors possessing different response kinetics. In the context of this work, the loss of adaptation occurs in the expression of PD-1 receptors on anti-melanoma CD8+ T cells, a phenomenon that may constitute the essence of the previously unrecognized immunologic factor (1), while competing push-pull factors (3) correspond to opposite outcomes of the corresponding kinetic motifs identified as incoherent feedforward loops (IFFLs) in the classification of Alon (6). We briefly note that push-pull factors also play multiple fundamental roles in physiology (and biology) in general, e.g., Dampney et al. (7).

Our working hypothesis is that the melanoma-specific T cells shunted to the lung in the presence of the infection express high levels of inflammation-induced cell-activation blocker PD-1, which upon interacting with PD-L1 constitutively expressed in the lung, render T cell motility paralysis (8). At the same time, virus-specific cells adapt to strong stimulation by their cognate antigen by lowering the transiently-elevated expression of PD-1, remaining functional and mobile while the infection is cleared.

Although other important mechanisms may contribute to the previously unrecognized acute non-oncogenic infection factor (1), we focus our efforts on one concrete aspect of the problem, which is a gene regulatory network (GRN) that controls PD-1 expression. Indeed, the fact that many other factors may contribute to the enormously complex molecular makeup of the acute non-oncogenic infection effect, such factors, obviously, do not exclude the interaction PD-1:PD-L1 playing a role as clearly seen from the data collected in Kohlhapp et al. (1). Thus, the importance of the PD-1:PD-L1 signal sent by the data cannot be disputed. Moreover, it is the PD-1:PD-L1 signal "detected" experimentally in Kohlhapp et al. (1) that defines the scope of our work aimed in uncovering relevant molecular detail in an unbiased way. We then develop and use a simple mathematical model in order to further illuminate the PD-1:PD-L1 role.

Specifically, a core component of our PD-1 gene-regulatory network (GRN) is a kinetic motif, which we call a Double Incoherent Feed-Forward Loop (PD-1 DIFFL), and which reflects known interactions between IRF4, Blimp-1, and Bcl-6 transcription factors (TFs). The different activity levels of the PD-1 DIFFL components, as a function of (a) the cognate antigen levels, (b) the T cell receptor (TCR) activity, and (c) the given inflammation context, manifest themselves in the T cell phenotypically distinct outcomes discussed in our work.

The rest of our work is organized as follows. In section 2.1, the main results of Kohlhapp et al. (1) are briefly outlined. Alternative hypotheses potentially related to the unrecognized factor are discussed in section 2.2. Here, the motivation for the development of the PD-1 DIFFL is also given. The PD-1 DIFFL is reconstructed in section 2.3. We next attempt to falsify and validate the kinetic motif (PD-1 DIFFL) against key experiential observations in section 2.4. The results of our mathematical modeling are described in section 2.5. Finally, a literature review of the corresponding mechanistic detail, the model construction, and the model's parameter justification can be found in **Supplementary Material**.

2. RESULTS

We begin our analysis of the experimental data (1) by discussing a few alternative hypotheses, followed by the introduction of a number of mechanisms consistent with the discussed observations.

The selected mechanisms will then be formalized in terms of a relevant genetic molecular circuit (PD-1 DIFFL) that regulates PD-1 expression. Our proposed PD-1 DIFFL model is based upon molecular detail discovered previously, and is independent of the results obtained in Kohlhapp et al. (1).

We hope that the strong inference methodological approach (9) that guides our research will allow us to customize the PD-1 DIFFL to different inflammatory conditions (1) with the ultimate goal to capture both infection-tumor and infection-infection interactions at the mechanistic molecular level.

2.1. Linking Observations With Immunological Mechanisms

A key challenge in the study of T cells within different dual immunological self (tumor) and non-self (infectious) contexts, is the organization of large amounts of relevant molecular and

biochemical information (section SI-1) compactly summarized in **Table 1**.

Specifically, **Table 1** highlights the following key observations (O1)–(O5) made in Kohlhapp et al. (1):

(O1) *Distant influenza-melanoma interaction:* Influenza-induced loss of anti-melanoma CD8+ T cells from the tumor micro-environment (TME) and their sequestration in the infected lung.

(O2) *The host immune system's ability to respond to concomitant infection challenges:* influenza A virus (IAV) infection does not impede clearance of vaccinia virus (VACV) infection under the same conditions, nor tumor challenge changes the ability of the immune system to eliminate the infection.

(O3) *Reactivation of exhausted (T_{EX}) anti-melanoma CD8+ T cells after anti-PD-1 (αPD-1) blockade:* (i) reactivated anti-melanoma CD8+ T cells which continue to reside in the TME regain their ability to contribute to the anti-tumor

TABLE 1 | A summary of the immunological reconstruction of infection-tumor interactions[a].

Observation	Description	Mechanism (hypothesis)
(O1) Anti-tumor CD8+ T cells are shunted to the infected site.	Tumor-specific CD8+ T cells of infected hosts were significantly reduced on day 6 in the TME compared to uninfected hosts and found at high levels at the site of infection but not observed in tissues unrelated to the tumor challenge or infection.	**(O1-M1)** Low-affinity immunological synapses formed between TCRs on anti-tumor CD8+ T cells and self-antigens on tumor cells lead to the lack of the Ag-induced arrest of the anti-tumor CD8+ T cells in the TME. **(O1-M2)** Infection-induced chemokines and cytokines amplify the tumor's ability to egress anti-tumor T_{EFF} from the TME. **(O1-M3)** Non-specific cardiovascular edema caused by infection-induced inflammation affects anti-tumor T_{EFF} trafficking. **(O1-M4)** Infection-induced chemokines chemoattract anti-tumor T_{EFF} to the infected lung. **(O1-M5)** Infection-induced IL-2 retains all types of T_{EFF} in the infected lung. **(O1-M6)** Infection-induced cytokines amplify expression of endothelial PD-L1, which in turn leads to paralysis of anti-tumor T_{EFF} in the inflamed lung due to PD-1:PD-L1 bonds.
(O2) Cancer does not suppress the immune system anti-viral response which is capable at the same time of eradicating concomitant infections efficiently.	Cancer does not alter significantly the natural clearance of infection. Influenza infection also does not alter the natural clearance of VACV or the proportion of VACV-tetramer+ CD8+ T cells at the site of influenza infection.	**(O2-M1)** High-affinity immunological synapses formed between TCRs on anti-infection CD8+ T cells and nonself-antigens on infected cells lead to the Ag-induced arrest of the anti-infection CD8+ T cells inside the infected sites until a full clearance of the infection antigen.
(O3) Therapeutic PD-1 blockade reverses infection-mediated anti-tumor response disruption.	PD-1 blockade decelerates tumor growth in influenza-infected mice as well as rescues the percentage of anti-tumor CD8+ T cells within the TME.	**(O3-M1)** αPD-1 blockade shifts the dynamic equilibrium of the dynamically formed PD-1:PD-L1 bonds toward unbound forms of both PD-L1 and PD-1, allowing anti-tumor T_{EFF} to recover from immunologic paralysis and to gain motility. **(O3-M2)** Due to αPD-1 blockade, reactivated anti-tumor CD8+ T cells may recirculate back to the TME with constitutive lymph motion. **(O3-M3)** αPD-1 blockade reactivates PD-1-blocked signaling pathways leading to (i) improved killing capability, (ii) proliferation, (iii) suppression of PD-1 expression, (iv) protection against exhaustion, etc. in reactivated CD8+ T cells.

[a] *Literature citations are directly inserted through the text (section SI-1).*

immune response and, additionally, (ii) reactivated anti-melanoma CD8+ T cells sequestered in the infected lung may regain their motility and return back to the TME, where they also aid in the anti-tumor response.

(O4) *Reduced host survival:* Infection early in tumor formation reduces host survival by promoting tumor growth in the infected host.

(O5) *Differential expression of PD-1 receptors by effector cells (T_{EFF}) in the infected lung:* Anti-melanoma CD8+ T cells express larger amounts of PD-1 receptors than anti-influenza CD8+ T cells under the same conditions in the infected lung.

2.2. From a Physiologic Systemic View of Lymphocyte Re-circulation to Systems Biology of PD1:PD-L1 Interactions

It is known (10, 11) that non-specific cardiovascular edema effects, caused by infection-induced inflammation in the infected site, redirect the blood-flow to the site of infection-induced inflammation. Therefore, it is highly appealing to explain the observed accumulation of anti-melanoma CD8+ T cells in the infected lungs, (O1), by non-specific inflammation effects only.

Note that the lymphocyte recirculation routes are phenotype-dependent and significantly differ for naïve/memory/effector subsets (12). We leave the corresponding details specific to the different subsets out of the discussion that follows. What is relevant to our work is that all newly activated cytotoxic T lymphocytes (CTLs) exit the corresponding lymph nodes into lymph via lymphatic ducts before they enter circulation via the great veins, and then flow through the pulmonary circulation (**Figure 1**). Under resting non-inflamed conditions, re-circulation of lymphocytes between lungs and blood is very rapid, with the average residence time in the lungs less than *one minute* (16).

After leaving the heart and lungs, the traveling CTLs continue to flow into systemic circulation, followed by their ultimate but not instantaneous homing in the corresponding infectious or tumor sites. Indeed, lymphocytes on average must pass via vasculature of the lung or liver about 10 times or even more times (15) before they migrate to one of the secondary lymphoid tissues (12)[BOX 14.2]. For example, it was shown that if anti-tumor CTLs were activated in the breast, they would perform on average about eight circulatory transient cycles before extravasation into the tumor site (15).

Before reconciling the experimental observation (O1) with these studies, we have to briefly discuss a unique role that the lung plays in the physiology and immunology of trafficking lymphocytes under both resting and inflamed conditions.

Experimental studies have revealed that different subsets of lymphocytes, including naïve/memory/activated effector T cells, transiently accumulate in the lungs (17, 18) both by means of and, what is also extremely important, without specific antigen-dependent recruitment of CTLs to the lung (19). Anderson et al. (19) further discuss "numerous observations indicating that T cell trafficking withing the lung is starkly different from what is known about T cell trafficking in most nonlymphid tissues,"

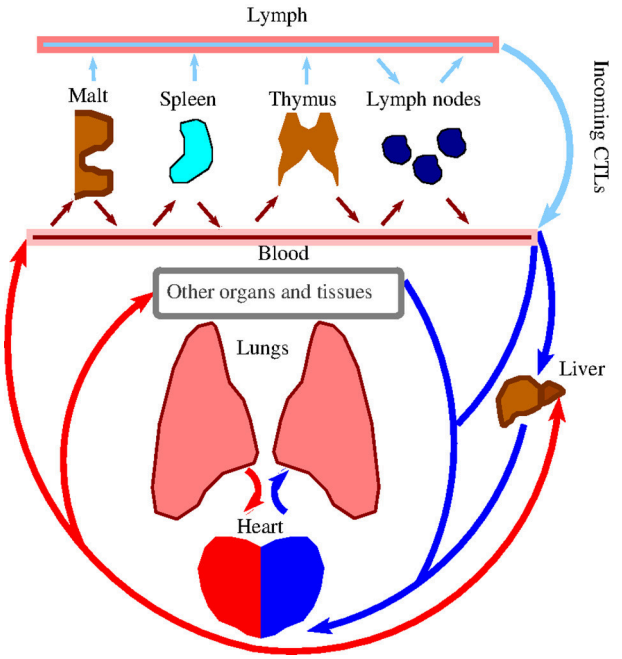

FIGURE 1 | Schematic representation of lymphocyte re-circulation routes. There are two different routes for naïve and activated trafficking lymphocytes (12, 13). First, due to the data discussed in Owen et al. (12, Ch.14) and, independently estimated in Van den Berg (14, p. 23) after approximately 30 min. transit time in the blood, about 45% of all naïve lymphocytes (produced by the thymus and bone marrow) migrate to the spleen, where they reside for about 5 h. Another 45% of lymphocytes enter various peripheral nodes, where they remain for 12–18 h, scanning stromal cell surfaces. A smaller fraction of lymphocytes migrate to secondary lymphoid tissues (skin, gastrintestinal, etc.), to protect the organism against the external environment. Thus, about 5% of the lymphocytes are, at resting conditions, in the blood, and the majority resides in the lymph nodes. Second, as discussed in Poleszczuk et al. (15) activated CTLs enter the blood system via the great veins, flow through the pulmonary circulation, and, then, continue into systemic circulation. Venus blood from gastrointestinal tract and spleen goes to the liver through the hepatic portal vein. In all cases, lymphocytes migrate from the blood into lymph nodes through high-endothelial venues, specialized areas in postcappillary venues. (a) MALT is Mucosa Associated Lymphoid Tissue. (b) Lymph nodes have both afferent and efferent lymphatic vessels, while MALT, Spleen, and Thymus have efferent lymphatic only (12).

including the fact that lymphocyte extravasation into the lung is chemokine independent (20, 21). So, one must revisit the observation (O1) by taking into account the unique role that the lung may play in lymphocyte retention even in the absence of influenza A related antigen-induced chemokine gradients that would additionally force anti-melanoma CTLs to extravasate into the lung epithelium, should influenza A infection be present.

Unfortunately, the above results and the unique role of the lung to transiently retain lymphocytes still do not explain the difference in the observations (O1) and (O2), nor they explain the observation (O3), for the following reasons.

First, concerning the observations (O1) and (O2), both anti-melanoma and anti-infection CTLs should follow the same pattern of multiple vascular re-circulation cycles as discussed above (**Figure 1**). However, under similar re-circulation patterns,

the presence of IAV infection impedes tumor clearance, while, at the same time, both IAV and another concomitant infection (e.g., VACV) are cleared efficiently as one infection would be cleared in the absence of another. Specifically, the question "Why are anti-melanoma CTLs retained in the infected lung, while anti-VACV infection CTLs are not?" remains unanswered.

Given the large literature body on the importance of PD-1 receptors in immune response and the observations (O3) and (O5), we decided to explore theoretically whether molecular signaling pathways initiated by PD-1 ligated with PD-L1 would provide at least one plausible mechanism to explain the results obtained in Kohlhapp et al. (1).

We have excluded PD-L2 from our model and only consider PD-L1 in the analysis that follows. Indeed, PD-L2 has restricted expression on macrophages, dendritic cells (DCs), and mast cells, while PD-L1 is expressed more broadly in order to mediate T cell tolerance in non-lymphoid tissues (12, 22). Besides, mathematical simulations based on the biophysical and expression data have revealed an unexpectedly limited contribution of PD-L2 to PD-1 ligation during interactions of activated T-cells with APCs (23).

To this end, the immune system has apparently evolved the inhibitory PD-1/PD-L1 pathway as a result of the need to control the degree of inflammation at locations expressing the antigen in order to secure normal tissue from damage and also to maintain peripheral tolerance (4, 22). This includes the constitutive expression of PD-L1 in large quantities in various tissues such as lungs, pancreatic islets, ovary, colon, etc. (24–29) by which cross-reactive effectors that survive positive selection are also muted to maintain the peripheral tolerance (2).

2.3. Incoherent Feed-Forward Regulation of PD-1 Expression

PD-1 expression on CD8+ T cells is known to be regulated at the level of transcription of its gene *pdcd1* (30). More precisely, two upstream conserved regulatory CR-B and CR-C regions (30) are key for PD-1 expression in response to CD8+ T cell activation. Specifically, TCR signaling induces PD-1 gene expression through the transcriptional activator, Nuclear Factor of Activated T cells, cytoplasmic 1 (NFATc1) (**Figure 2**), which binds to CR-C after translocation to the nucleus (30, 31).

Next, the down-regulation of PD-1 during acute infection (32) suggests that there exists a mechanism that directly represses its expression after initial activation events. Indeed, Blimp-1 (B Lymphocyte-Induced Maturation Protein 1) (33) has been found to be induced during the *later* stages of CD8+ T cell activation and was shown to be required for the efficient terminal differentiation of effector CD8+ T cells (30). When Blimp-1 is suppressed, the same data suggest that in the absence of Blimp-1, PD-1 expression is maintained by NFATc1 (**Figure 2**).

For the sake of completeness, we recall that the existing data also suggest that Blimp-1 represses PD-1 gene expression in CD8+ T cells using three distinct molecular mechanisms (30):

(1) regulation of the expression of PD-1's activator NFATc1;
(2) alteration of the local chromatin structure; and

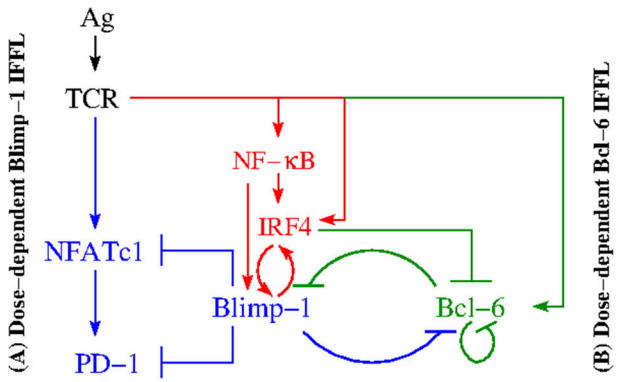

FIGURE 2 | Regulation of PD-1 expression. Two different IFFLs, sharing a common set of species and regulatory activities highlighted in red, are presented. Both IFFLs are activated by the same input (Ag). The left hand side **(A)** depicts a dose-dependent biphasic activation of PD-1. The elements of the corresponding IFFL are highlighted in blue and red colors. When the input, the Ag dose, increases, the output, the PD-1 level, first also increases but then subsequently decreases. The right hand side **(B)** corresponds to a dose-dependent activation of Bcl-6. The elements of the corresponding IFFL are highlighted in green and red colors. Over a certain range of input dose, the Ag level, the output, in this case Bcl-6 level, increases but with a subsequent increase in the Ag dose, the Bcl-6 level then decreases.

(3) eviction of the activator NFATc1 from its site that controls PD-1 expression.

In addition, Blimp-1 has been found to be a transcriptional antagonist of proto-oncogene Bcl-6 (B cell lymphoma 6 transcription factor), and vice versa (**Figure 2**) (i.e., Blimp-1 and Bcl-6 are known to mutually repress one another) (34–38). Specifically, Blimp-1 can bind to the *bcl6* promoter (39).

Although it is not known exactly how Bcl-6 inhibits Blimp-1 in T cells, it is well known that in B cells Bcl-6, in association with a corepressor MTA3, represses *prdm1* by binding to sites in *prdm1* intron 5 and intron 3 (34, 40, 41). We take this fact into consideration because signaling pathways and their activation are similar in both B and T cells (12). Additionally, Bcl-6 binds its own promoter and inhibits its own transcription (**Figure 2**), thus implementing an autoregulatory loop (42, 43) (**Figure 2**).

Competing with Bcl-6 for intron 5 in *prdm1*, IRF4 (Interferon Regulatory Factor) (44–47) is shown to be a direct activator of *prdm1* (**Figure 2**) by binding to a site in intron 5 (34). At the same time, IRF4 directly represses gene *bcl-6* by binding to a site within its promoter (34, 45), which is rich in IRF4-binding sites (43).

Because IRF4 is known to be activated both directly via TCR and by NF-κB (48, 49), we have then sought to determine who activates NF-κB in this context and found that NF-κB is activated by TCR signaling (34, 37, 50, 51). Several potential NF-κB binding sites in the *prdm1* promoter have been suggested. It is also known that IRF4 can bind to its own promoter, supporting a positive feedback mechanism by which high IRF4 expression can be maintained (43, 52).

There are additional signaling routes leading to the activation of IRF4 (e.g., via Akt-mediated pathways) which are not discussed here (34).

After a careful analysis of the reconstructed molecular interactions, we have come to the conclusion that this intricate reaction network consists of two subnetworks (**Figure 2**). Both subnetworks have the same input from the activated TCR, while the outputs of the subnetworks are different. Namely, PD-1 is the output of the subnetwork color-coded in blue and red, while Bcl-6 is the output of the subnetwork color-coded in green and red. The two subnetworks share a number of common species and interact with one another via repressive interactions mediated by the three key species color-coded in red, (i) IRF4, (ii) Blimp-1, and (iii) Bcl-6.

Each of the two subnetworks corresponds to a gene-regulatory network (GRN) motif known as an incoherent feed-forward loop (IFFL) (6). Because the PD-1 circuit is formed of two such IFFLs, we call it a Double Incoherent Feed-Forward Loop (DIFFL).

Our IFFL network may be viewed as a mechanistic instantiation of a conceptual signal discrimination model based on a competition between "excitation" and "de-excitation" factors possessing different response kinetics, as initially introduced by Grossman and Paul (3). The latter concept has been gradually applied successfully in multiple studies since 1992 as reviewed in Grossman and Paul (5). In that sense, we address with our model the following goal formulated in Grossman and Paul (3): "More explicit rules of organization, or models, need to be explored. Such rules should suggest, in particular, how the functional segregation of immunological responses may reasonably come about."

2.4. PD-1 Expression Within Different Inflammatory Contexts

We next attempt to validate the PD-1 DIFFL motif (**Figure 2**) against all observations reported in Kohlhapp et al. (1) by following the falsification and validation methodology (53), which is also fundamental to any modeling study. **Figure 3** will be instrumental in our analysis that follows.

Figure 3A shows a biochemical reaction network reconstruction customized for the case of an anti-influenza cytotoxic effector T cell, T_{EFF}, in the presence of large amounts of cognate Ag in the infected lung. In this case, the immunological complexity of interactions involving cytokines is already overwhelming (5, 54–58). For example, IL-2 activates and is simultaneously repressed by active Blimp-1 both directly and indirectly (31, 59).

The abundance of the cognate viral Ag in the infected lung leads to a strong TCR activation which, in turn, results in the simultaneous activation of Blimp-1 and degradation of Bcl-6 (section 2.3) followed by suppression of PD-1 transcription with its subsequent degradation. The biochemical detail can explains transient and rapid PD-1 expression followed by downregulation of PD-1 expression in the presence of acute infection (32), see also section SI-1.2.

All this may also explain why anti-infection CD8+ T cells are not exhausted during the first phase of the biphasic response of the PD-1 DIFFL-circuit (section 2.3) despite the fact that bystander and tissue cells express large amounts of PD-L1 caused by large concentrations of pro-inflammatory cytokines such as INFγ (SI-1.1). Recall that large amounts of PD-L1 are already constitutively expressed in the lung under resting condition in the absence of any infection (section 2.3).

Figure 3B shows the response of the reconstructed circuit in the tumor microenvironment (TME). Specifically, anti-melanoma CD8+ T cells overexpress PD-1 in the presence of large amounts of tumor-specific cytokines such as IL-6, a well-described regulator of Bcl-6 expression (38). Due to relatively low levels of tumor Ag and a weak self-Ag TCR signal (60) of anti-tumor CD8+ T cells, the TCR is not activated strongly enough to activate Blimp-1 and, at the same time, the weak activation of the TCR sets the first phase of the biphasic response of the dose-dependent PD-1 DIFFL motif (**Figure 2**).

Indeed, the PD-1 DIFFL strongly activates Bcl-6 for small and medium TCR strengths, and weakly activates Bcl-6 for high activity levels of TCR. As a result, Bcl-6 is overexpressed, while Blimp-1 is not expressed in the melanoma TME (38), which leads to the overexpression of PD-1 on the surface of anti-tumor CD8+ T cells.

Figure 3C shows the PD-1 DIFFL in an anti-melanoma T_{EFF} relocated into the infected lung. In this case, the conditions discussed just above to introduce **Figure 3B** play the role of a spark plug that activates the transcription of Bcl-6, which represses *prdm1* even after the relocation of the anti-tumor T_{EFF} into the lung.

These relocated T_{EFF} can now sense the elevated levels of INF-γ and TNF-α, which are abundant in the infected site, and which are produced by professional antigen presenting cells (APCs) (section 2.2).

The cytokines strongly stimulate the expression of both PD-1 and PD-L1 (61), as well as maintain the expression of PD-1 on the surface of the anti-melanoma T_{EFF}, initially sparked by the ligation of TCRs with cognate tumor Ags during the time when the T_{EFF} cells were present in the TME before their relocation to the lung.

Because the tumor Ag is absent from the infected lung, the TCR is not ligated, and, hence, all routes leading to the activation of Blimp-1 and IRF4 are disabled. We can thus propose that the major route contributing to PD-1 overexpression here is mediated by INFγ and TNFα. The corresponding PD-1 expression activation route is marked by sign + inside a circle in **Figure 3C**.

Recall that large quantities of PD-L1 are constitutively expressed in the lung already under resting conditions (section 2.2). PD-1 mediated control of immune responses depends on interactions between PD-1 on CD8+ T cells and PD-L1 in tissues (62). Importantly, such PD-1:PD-L1 interactions can result in CD8+ T cell motility paralysis (8, 28, 63).

We introduce the paralysis mechanism (**Figure 4**) in detail in (O1-M6) (section SI-1.3) and believe that this mechanism can provide a valuable insight into the previously unrecognized factor contributing to the retention of anti-melanoma CD8+ T cells shunted to the influenza A infected lung (1). Of course, other yet unknown mechanisms may exist and need to be elucidated in order to provide a more complete explanation of the retention effect (1). Therefore, additional experimental observations should be obtained.

The study conducted by Cheng et al. (23) reports that "it now seems that very stable complexes are not prerequisite for potent inhibitory PD-1:PD-L1 signaling" because measurements of the human and mouse PD-1 binding to PD- L1 affinities suggest that potent inhibitory signaling can be mediated by weak interactions.

Zinselmeyer et al. (8) further stress: "Prolonged motility arrest is an excellent host strategy to decrease T cell efficiency and likely facilitates exposure to multiple regulatory pathways. PD-1:PD-L1 blockade is known to restore function to virus-specific and tumor-specific T cells, and has shown some promise in recent clinical trials."

Although dissociation and association of the complex PD-1:PD-L1 are assumed to be fast (64, 65), this however does not preclude the long-known loss of T cell motility due to multiple PD-1:PD-L1 interactions (66, 67).

Figure 3D shows the PD-1 DIFFL in an anti-melanoma T_{EFF} cell in the infected lung after administration of PD-1 (αPD-1) blockade. Recall that the NF-κB pathway is downregulated in exhausted CD8+ T cells (38). To this end, the PD-1 blockade (marked by symbol αPD-1 color-coded in red) in **Figure 3D**, removes the brake (68) from the corresponding T cell signaling pathways (see section 2.1, observation O(3), and **Table SI-1.1**) leading to overexpression of NF-κB (66, 69). Additionally, NF-κB activation is positively regulated through TNFR (TNF Receptor) and TLR (Toll-like Receptor) sensing TNFα and viral materials in the infected lung, respectively (70–72).

As discussed earlier, NF-κB activates IRF4 (34), and the latter directly represses Bcl-6 (34). In turn, the repression of Bcl-6 removes the brake from the overexpression of Blimp-1, which then leads to reduced numbers of PD-1 receptors on the surface of reactivated anti-melanoma effector cells. This may allow the reactivated T_{EFF} to become mobile (**Table SI-1.1**) with a potential to relocate back to the melanoma TME with the lymph flow and blood circulation as discussed in the mechanism (O1-M6). Indeed, it is well known that after the T_{EFF} re-circulation in the blood (15), effector T cells are preferentially found in the lymph nodes in which their activation occurred, and in the area drained by those lymph nodes (73).

The above conclusions are also based on the experimental evidence that PD-1:PD-L1 interactions contribute to reduced T cell motility on day 7, and therapeutic blockade of PD-1:PD-L1 restore CD8+ T cell motility within 30 min (8). Although we use the references (8, 63) in order to support our hypotheses, additional experimental research is needed to understand deeper the paralysis phenomenon (28, 63).

We conclude our discussion of the PD1 DFFIL motif by noting that the core of the reconstruction (**Figure 2**) fits well to all discussed inflammatory contexts (**Figure 3**).

2.5. Probing Immunobiochemical Reconstruction Modeling

Our modeling goal here is quite simple. Given the discussed specificity of PD-1 expression (section 2.4) with respect to different amounts of antigen available in the medium and different values of TCR affinity in terms of the values of the off-rate constant k_{off} for the Ag:TCR bond (74, 75), we focus on the analysis of the dependence of the levels of key species, Bcl-6, IRF4, Blimp-1, and PD-1, on the two parameters, (i) the antigen concentration, Ag, and (ii) the values of k_{off} defined in sections SI-2 and SI-3.

2.5.1. Modeling PD-1 Expression in the Absence of PD-L1

We first consider the case when the PD-1:PD-L1 interaction is absent from the model by setting $\phi_L(P) \equiv \Phi(P) \equiv 1$ corresponding to the condition $L = [\text{PD-1:PD-L1}] = 0$ in both Equations (SI-2.1c) and (SI-2.2a).

Typical plots for the (non-dimensional) steady-state (76) concentration levels of PD-1, Bcl-6, Blimp-1, and IRF4 in the absence of the PD-1:PD-L1 interaction and at the different values of k_{off} are shown in **Figure 5**. The model's nondimensionalization is done in sections SI-2 and SI-3.

We next discuss the case of small values of k_{off} from the set of the values given in the legend of **Figure 5**. We observe from **Figure 5** that the level of PD-1 (**Figure 5A**) becomes rapidly elevated already at very small values of the scaled Ag-concentration (section SI-1). A further increase in the scaled Ag-concentration results in the formation of the PD-1 level plateau, followed by a drop in PD-1 levels.

The increase in the level of PD-1 (**Figure 5A**) is fully aborted when the level of Blimp-1 (**Figure 5C**) reaches the threshold sufficient to suppress PD-1 expression initiated by TCR activation. We interpret the top (left) plateau in the level of PD-1 (**Figure 5A**) as corresponding to the homeostasis maintained by both the PD-1 DIFFL and the negative feedback activation of TCR which we discuss shortly below. At the same time the bottom (right) plateau in the level of PD-1 (**Figure 5A**) can be interpreted as an adaptation to high levels of Ag (3), a direct consequence of adaptive properties of IFFLs (6, 77–82).

We further observe that in complete agreement with the theory of IFFLs demonstrating biphasic steady-state behavior (6, 77, 78), the levels of Blimp-1 and IRF4 first increase and then decrease, and, at the same time, the level of Bcl-6 first decreases and then increases, while the level of Ag is constantly increased. Remarkably, the levels of all the three species almost perfectly adapt to their respective original states formed initially at very low levels of Ag, when the level of Ag becomes high enough to establish adaptation. A similar adaptive phenotype is discussed using an example of a generalized enzyme network in Chiang et al. (79).

Consider now the case of large values of k_{off} from the set of the values given in the legend of **Figure 5**. In this case, the response of the PD-1 DIFFL becomes abnormal, when all remarkable adaptive properties are completely lost. Even in the case of a very large value of k_{off}, the model predicts a tonic expression of PD-1 corresponding to very small nonzero values coded in black color in **Figure 5A**. We believe that this tonic expression of small PD-1 levels can be attributed to the immune tolerance discussed in section SI-1.

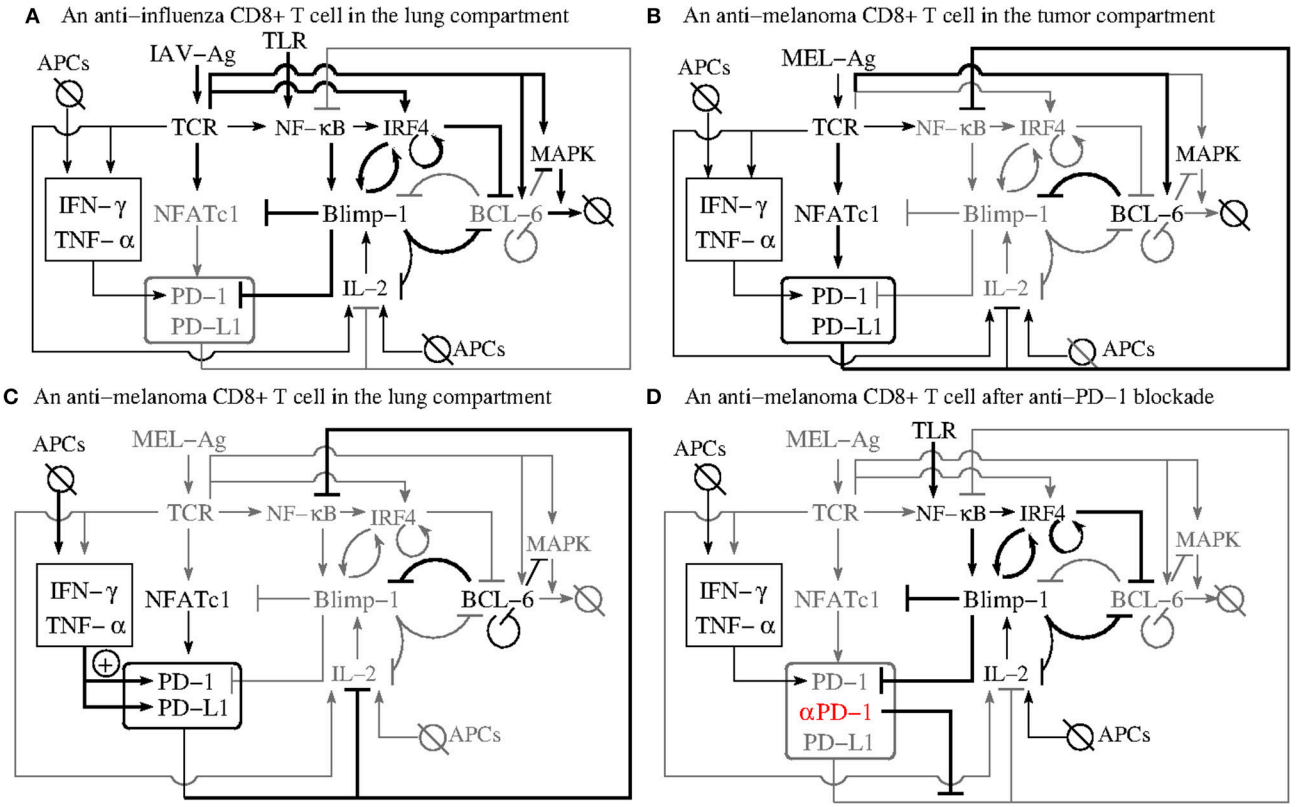

FIGURE 3 | The PD-1 DIFFL motif in the context of complex influenza-tumor interactions. **(A)** Shows the PD-1 DIFFL response in an anti-influenza CD8+ T cell in the infected lung. **(B)** Shows the response of the PD-1 DIFFL circuit in an anti-tumor CD8+ T cell in the TME. **(C)** Shows the PD-1 DIFFL response in an anti-tumor CD8+ T cell in the influenza-infected lung. **(D)** Shows the PD-1 DIFFL response in an anti-tumor CD8+ T cell in the influenza-infected lung after PD-1 blockade. Gray color corresponds to weak or disabled reactions shaped by the given inflammation context. Symbol + inside a circle in **(C)** shows the additional PD-1 activation route initiated by external cytokines in the case when the Blimp-1 mediated repression of PD-1 expression is absent. This route does not play any significant role in the case when the expression of PD-1 is suppressed by active Blimp-1 as in **(A)**. Arrows denote activation, and barred lines denote repression. The abbreviation APCs stands for (influenza) Antigen Presenting Cells.

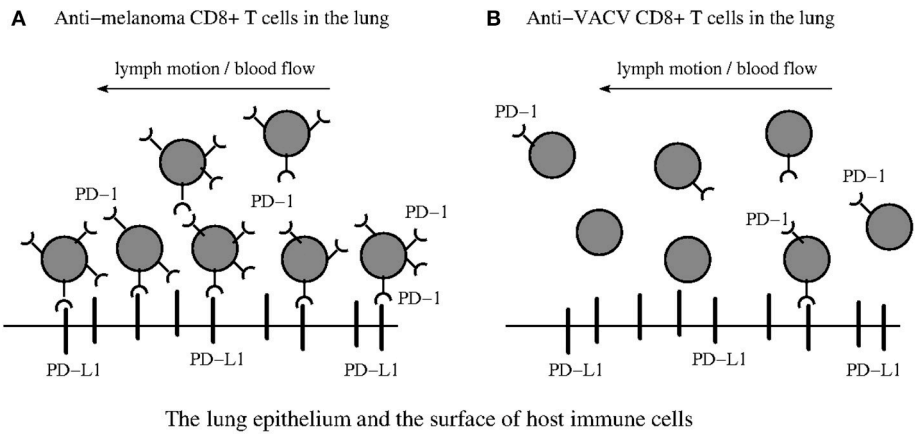

FIGURE 4 | PD-1:PD-L1 induced paralysis of the anti-tumor exhausted CD8+ T cells in the infected site. **(A)** Suggests that anti-melanoma T_{EFF} cells become paralyzed in the infected lung. In contrast, **(B)** suggests that anti-VACV T_{EFF} studied in Kohlhapp et al. (1) can freely enter and leave the infected lung with the lymph motion and blood flow due to the lack of large amounts of PD-1 receptors on their surface. The immune suppressive environment (4) induced by inflammation in the infected lung is caused by multiple interactions between PD-1 receptors, expressed in large quantities on the surface of the anti-melanoma T_{EFF}, and the PD-L1 ligands expressed in large quantities on the surface of various host immune cells (macrophages, DCs, and MDSCs) and the epithelium (29).

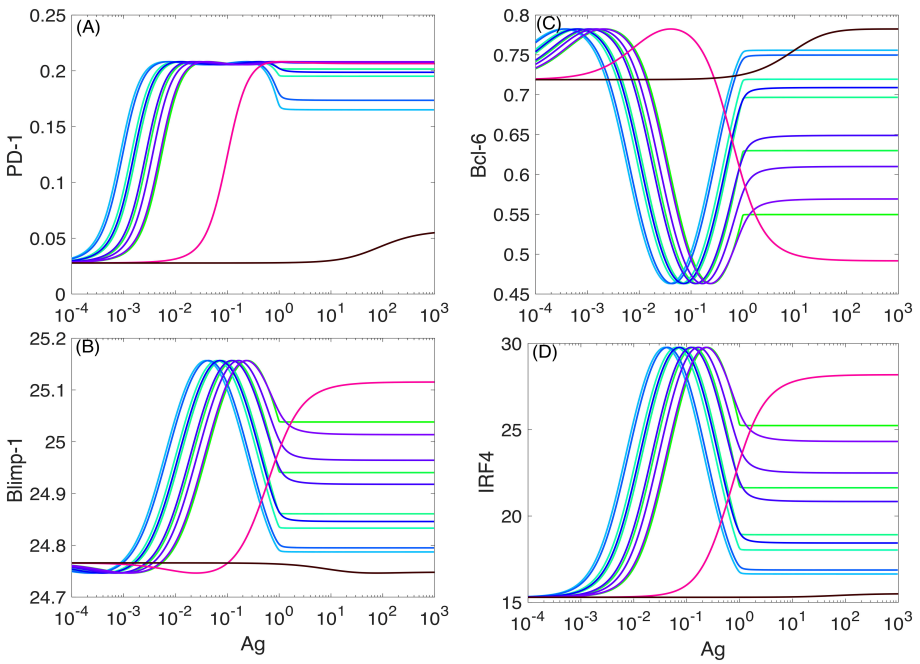

FIGURE 5 | PD-1 DIFFL responses in the absence of PD-1:PD-L1 interaction. The color-coded plots corresponds to the PD-1 DIFFL-induced adaptation with respect to increasing Ag-levels. To obtain a full adaptation, approximately a 10^3-fold increase in the Ag-level is required. Four different (bottom-up) shades of green color correspond to $k_{off} = 10^{-4}$, 2.03×10^{-4}, 4.13×10^{-4}, and 5.88×10^{-4}, respectively. Two shades of blue color correspond to $k_{off} = 2.43 \times 10^{-3}$ and 7.01×10^{-3}, respectively. Four (top-down) shades of purple color correspond to $k_{off} = 2.03 \times 10^{-2}$, 4.13×10^{-2}, 5.88×10^{-2}, and 8.38×10^{-2}. Magenta color corresponds to $k_{off} = 1.0$. Black color corresponds to $k_{off} = 49.24$. **(A–D)** Correspond to the levels of four species, PD-1, Blimp-1, Bcl-6, and IRF4, computed from the model developed in SI2, respectively.

To better see the role of IFR-4 and its impact on the level of PD-1, we then completely disabled IRF4 by setting the value of the parameter k_b to zero, $k_b = 0$ in the Equation (SI-3.1d). This computational experiment can be thought of as an "*in silico* IRF4-knockout." The corresponding plot of PD-1 levels against the Ag-concentration is shown in **Figure 6A**.

Surprisingly, the shapes of all PD-1 level plots obtained for the same set of k_{off} values as in **Figure 5** are preserved, and only the magnitudes of the corresponding levels are changed by a factor of 40 or more.

Motivated by these computational predictions, we checked if IRF4 knockout results were previously reported in the literature and found that *irf4*-deficient CD4+ T cells display increased expression of PD-1 associated with T cell dysfunction (83, 84). However, the role of IRF4 is still poorly understood as it can be completely opposite in the cases of acute and chronic infections (83, 85).

The second interesting observation (**Figure 6B**) is that while the PD-1 DIFFL regulatory function is lost due to *in silico* knockout of IRF4, the adaptation of PD-1 expression with respect to Ag levels (**Figure 6A**) is still preserved by the negative feedback regulation of TCR activity (**Figure 6B**) (5, 86–88). Both the TCR activation and the negative feedback are interpreted as another IFFL in Lever et al. (74). Collectively, we can thus conclude that the PD-1 transcription and its adaptation to high levels of antigen is regulated by multiple incoherent feed-forward loops.

2.5.2. Modeling PD-1 Expression in the Presence of PD-L1

We observe that in the presence of PD-1:PD-L1 interactions, the maximum levels of PD-1 and Bcl-6 increase (by a factor of 6.75 and 7.86, respectively, but, of course, these numbers are only meaningful in our model and with the parameters used, and they do not have biological significance) (**Figure 7**). At the same time, the levels for Blimp-1 and IRF4 are negligibly small, which allows us to interpret that the transcription of these two species is almost fully suppressed (**Figure 7**).

From our comparison of the PD-1 level plots in **Figures 5**, **7**, we can conclude that the PD-1:PD-L1 interaction plays the role of an amplifier of transient activation of PD-1 transcription, initiated by the ligation of TCR with Ag presented with an MHC (section SI-1).

PD-1:PD-L1 interactions may terminate signal transduction pathways, including those pathways that lead to the activation of IRF4 and Blimp-1, by recruiting phosphatases (68, 89, 90).

Our last computational experiment compares quantitatively the PD-1 level on the surface of an anti-melanoma CD8+ T cell shunted to the lung with the PD-1 level on the surface of an anti-influenza CD8+ T cell in the lung under the same conditions.

To conduct the computational experiment, the following conditions were taken into consideration: (i) the absence of distant tumor Ag in the lung, leading to the shutting down of the TCR signal ($U = 0$ in the Equations (SI-2.1a–d), (ii)

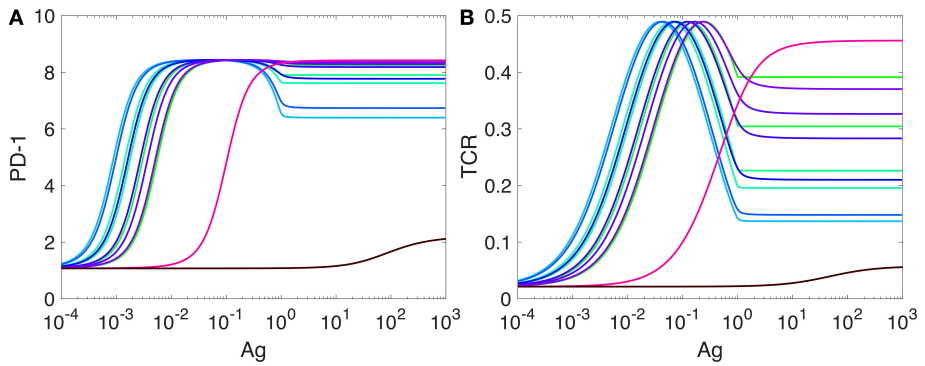

FIGURE 6 | Expression of PD-1 in the case when the expression of IRF4 is disabled. The levlel of PD-1 receptors in **(A)** is computed from our model developed in SI2. The level of TCR activity in **(B)** is computed from the model developed in Lever et al. (74) as explained in SI-2. All other explanations and parameter values are as in **Figure 5**.

the abundance of inflammatory cytokines, including TNFα and IFNγ, known to induce the expression of both PD-1 and PD-L1 (SI-1), and (iii) the abundance of IL-2, which induces Blimp-1 (SI-1).

To account for the abundance of the lumped TNFα and IFNγ species, we have replaced the rate constant σ_p in the Equation (SI-2.1b) by the rate expression (SI-2.6). To account for the abundance of IL-2 in the lung compartment, we have increased the value of the parameter a_b by a factor γ in Equation (SI-2.1d). In this case, we assumed that IL-2 was secreted by activated T cells (50) and, hence, IL-2 affected Blimp-1 expression through autocrine and paracrine signaling, depending on the TCR activation strength.

In the case when the value of the parameter γ was set to one, the level of PD-1 was increased by a factor of 6 compared with the maximum level of PD-1 shown in **Figure 7** for both anti-influenza and anti-melanoma cases. So, we can conclude that just the PD-1 DIFFL alone is not enough to counteract the effect of the pro-inflammatory cytokines. Only when a "strong action of IL-2" was taken into consideration by setting $\gamma > 5{,}000$, the level of PD-1 was suppressed for anti-influenza T cells.

3. DISCUSSION

Below we discuss our modeling studies conducted in order to complement our immunobiochemical reconstruction toward a better understanding of the previously unrecognized acute non-oncogenic infection factor (1). We then discuss potential implications of our research to further stimulate ongoing efforts toward developing and improving physiological and functional cure approaches based on the host's ability to eliminate non-self foreign invaders and, at the same time, the host's inability to install strong altered-self (cancer) responses (2).

3.1. What We Learn From the Model

Our PD-1 DIFFL reconstruction (**Figure 2**), when combined with the mathematical modeling (**Figures 5**, **7**), suggests that it is the loss of Ag dose-dependent adaptation of the expression of PD-1 receptors in the anti-tumor CD8+ T cells that could be one of major factors resulting in the multiple effects in the presence of acute non-oncogenic infection (1). Specifically, in the case of acute infection, the level of PD-1 receptors on the surface of Ag-experienced anti-infection CD8+ T cells first increases and then decreases to lower levels in the course of the virus replication (**Figure 8B**), the hallmark of a fundamental biological adaptation (3). Therefore, based on the discussion around **Figure 3**, we can conclude that chances that the cells with the phenotype shown in **Figure 8B** will loose their motility due to PD-1:PD-L1 interactions in the infected lung are low (**Figure 4**).

In contrast, in the case of Ag-experienced anti-tumor CD8+ T cells, due to the much smaller levels of tumor antigens presented with MHCs in the TME, the strength of the TCR signal in anti-tumor CD8+ T cells may not be enough to activate Blimp-1 and IRF4 species to suppress PD-1 expression (**Figures 2**, **3**). The lack of the expression of Blimp-1 in melanoma is known experimentally (38). As a result, chances that T cells bearing large numbers of PD-1 receptors (**Figure 8A**) will be paralyzed in the infected lung due to PD-1:PD-L1 interactions are high.

Importantly, the higher levels of PD-1 receptors on anti-melanoma CD8+ T cells compared with much lesser levels of PD-1 receptors on anti-influenza CD8+ T cells co-localized in the same infected lung were observed in Kohlhapp et al. (1). This supports the two different phenotypes shown in **Figures 8A,B**, respectively.

Our quantitative estimates obtained from the model (**Figures 5**, **7**) show that the Ag level should be increased by several orders of magnitude required to move the Ag-experienced T cell from phenotype (A) to phenotype (B) (**Figure 5**). This means that at least a 1000-fold increase in cognate Ag levels (**Figures 5**, **7**) may be required for the adaptation of PD-1 expression to strong antigen-mediated stimulation.

Although more research into the novel adaptation effect illuminated by our model as well as into the lymph motion (93, 94) and molecular mechanisms by which cells are rapidly moved with the blood (95) is undoubtedly needed, we believe that it is worth providing some "biological" numbers that support

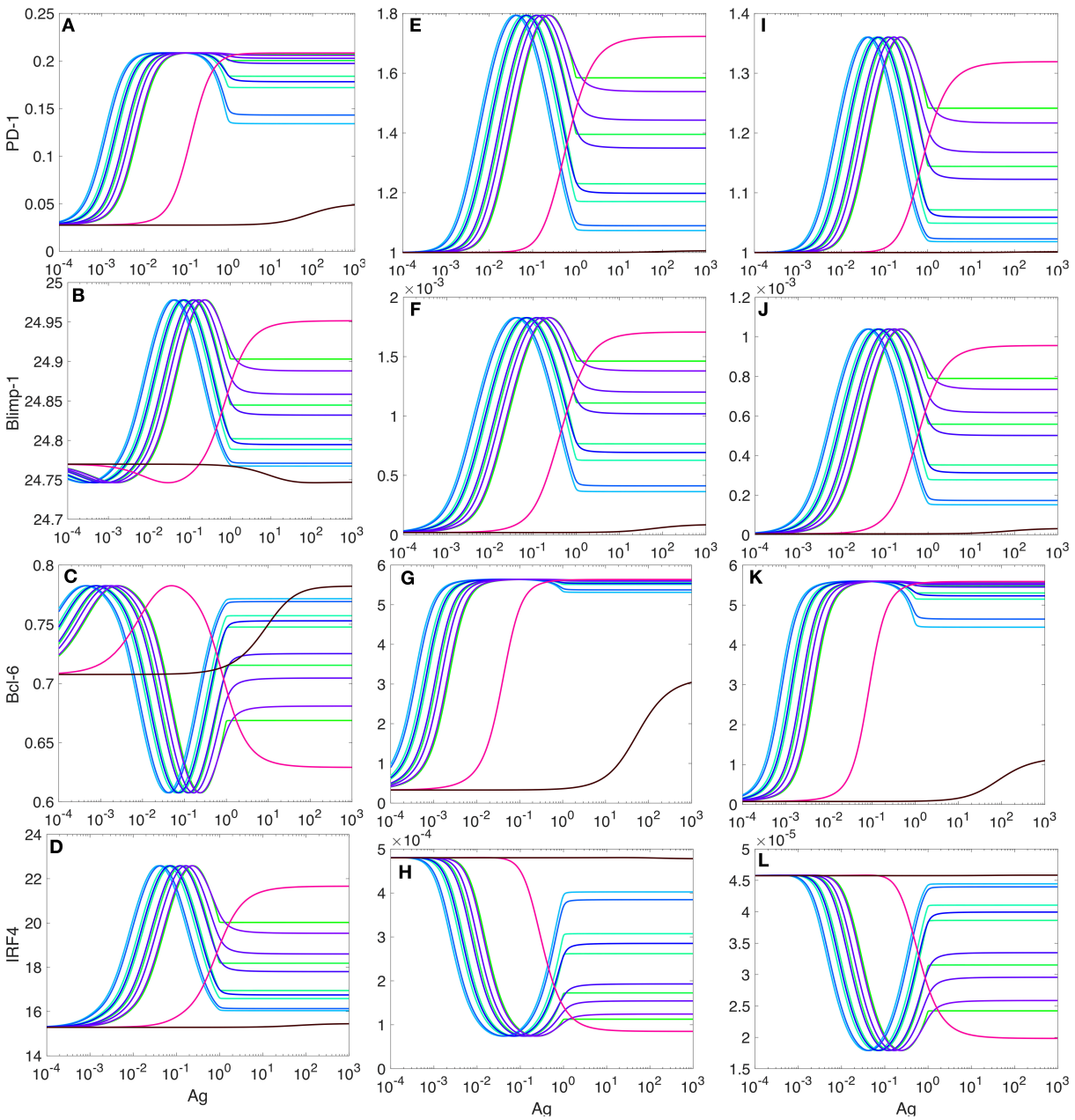

FIGURE 7 | PD-1 DIFFL responses in the presence of PD-1:PD-L1 interaction. **(A–D)** Correspond the case when 20% of PD-1 receptors are ligated with PD-L1. **(E–H)** Correspond the case when 50% of PD-1 receptors are ligated with PD-L1. **(I–L)** correspond the case when 90% of PD-1 receptors are ligated with PD-L1. All other explanations are provided in the legend for **Figure 5**.

our findings. For example, for the LCMV system, a gold standard for infectious biology, the virus titer was increased by factor about 10^3 from day 2 to day 5 (92, Figure 4.4). We digitized the corresponding data points and plotted them in **Figure 8** next to **Figure 8B**. Similar data are reported for influenza A infection (96, 97). The examples of the population measurements are well translated to our modeling studies because in all cases we use dimensionless ratios of the corresponding concentrations.

Of course, one also needs to make sure whether a T cell would be capable to provide a large number of TCRs sufficient to accommodate the above huge increase in Ag-levels. Indeed, the typical number of TCR molecules is estimated in the range of 3×10^4 (98), which is a reasonable number to match up with the model-suggested transition from phenotype (A) to phenotype (B) shown in **Figure 8**. At the same time it is highly unlikely for tumor cells to divide as fast as the viruses do to build enough antigen that would be sufficient to change phenotype (A) to

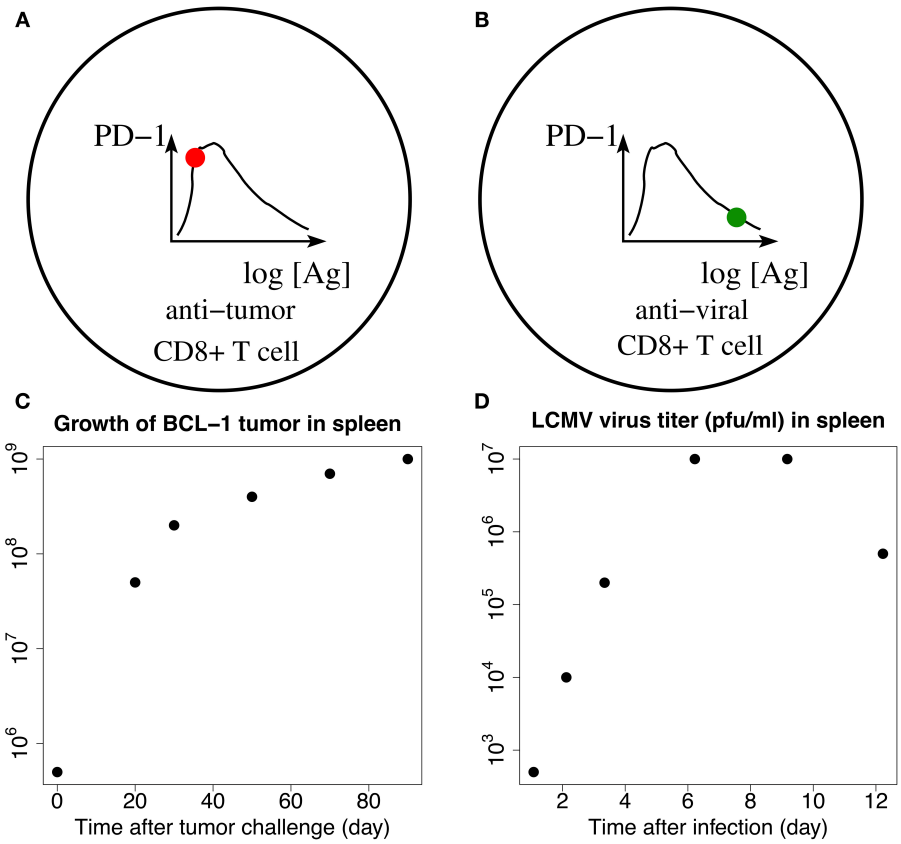

FIGURE 8 | Schematic illustration of the adaption loss/gain hypothesis. Solid filled circles on the corresponding graphs of PD-1 receptor levels (top panels), plotted vs. the log-concentrations of Ag, correspond to the levels of PD-1 receptors on anti-melanoma **(A)** and anti-virus **(B)** CD8+ T cells, respectively (top panels). Phenotype **(B)** corresponds to a fully developed adaptation of the PD-1 expression with respect to the increasing levels of Ag, while phenotype **(A)** is characterized by the lack of such adaptation. Bottom **(C,D)** show time-dependent levels of BCL-1 tumor cells (left) and LCMV virus titers (right) in the spleen. The data points are digitized from the corresponding plots in Kuznetsov et al. (91) and Bocharov et al. (92), respectively. Comparing **(C,D)**, we observe that the changes in the tumor Ag levels within the first 7 days are small, corresponding to the fold change less than 10 as seen from **(C)**. At the same time, the viral Ag levels change significantly, corresponding to the 10^4-fold increase during the first seven days as seen from **(D)**. The small 7-day tumor Ag-level increase shown in **(C)** corresponds to the red solid "snapshot" circle in **(A)**, while the large 7-day increase in the viral Ag level shown in **(D)** corresponds to the green solid "snapshot" circle in **(B)**. Additional detailed explanations of **(A–D)** are provided in the main text.

phenotype (B) within a few days. Indeed, the doubling time for virus particles can be 43–65 min (99), while the doubling time for malignant mouse melanoma B16 cells may take up to 2.8 days or longer (100, 101).

To support the above argument, we note that (91) uses experimental data where the number of tumor cells is increased by factor about 10^2 in the time span of just 40 days. We digitized the corresponding data points and plotted them in **Figure 8** next to **Figure 8A**. We can thus conclude that due to our modeling estimations (**Figures 5**, **7**), such a slow increase in Ag levels may not be enough to change between the prototypes shown in **Figure 8** for short periods of time (days), when acute infection develops and is cleared (1). Similar data can be learned from other independent studies (102).

Note that the discussed transient elevation of PD-1 receptor levels as function of antigen, **Figures 8A,B**, was experimentally observed and was also used as a "window of opportunity" in the context of the combined radiotherapy (RT) and anti-PD-1:PD-L1 treatments (103). Our theoretical work provides additional valuable insight into, and add in the development of combined RT/anit-PD-1:PD-L1 therapy.

3.2. Harnessing Anti-infection and Anti-bacterial Responses Against Cancer

By addressing the "the previously unrecognized acute non-oncogenic infection factor" revealed through systematically collected heterogeneous experimental data encompassing different pathogens and tumor types (1), we have suggested and discussed concrete molecular mechanisms which allowed us to delineate inherently weak anti-cancer (i.e., altered-self) immune responses from inherently strong anti-infection (i.e., non-self, foreign) responses, including co-infections.

Our findings may thus have potential clinical relevance particularly in the context of ever-expanding immunotherapy efforts and FDA approvals involving PD-1/PD-L1 axis immune checkpoint blockade. Two relevant scenarios to consider, include

(1) that patients with cancer treated with such blockade may also be experiencing a concomitant diagnosed or sub-clinical undiagnosed infection in a tissue distant to their tumor, and (2) that selective patients with cancer are being treated with oncolytic viruses (OVs), which preferentially infect tumor cells, but can also infect cells in tissues distant to their tumor (104, 105). In both scenarios, checkpoint blockade may have less-recognized effects discussed here (e.g., releasing the T cell motility paralysis caused by an infection in a tissue distant to the tumor) and thus such blockade may improve patient outcomes, including in the context of combination with OVs (106). As additional clinical information is collected from patients receiving checkpoint blockade (including about infection status and OV viral loads in non-injected sites), future efforts may provide the data necessary to reveal and model this blockade effect further.

We conclude this work with a hope that our theoretic analysis of the newly discovered infection-tumor interaction (1), made by combining solid immunobiochemical reconstruction with appropriate mathematical modeling may also be useful in current developments of both "physiological" and "functional cures" (2). Specifically, our mechanistic molecular-based analysis of the novel immunologic phenomenon uncovers important competing push-pull processes fundamentally inherent in immunity (3–5). We believe that the results reported may have broader implication toward developing (i) *physiological cure* approaches in order to completely eliminate tumors as it happens in the case of rapid (one week long) clearance of acute infection, and, alternatively, toward undertaking (ii) *functional cure* treatments to maintain long-term immunologic control as in the cases of controlled chronic infection and other disorders as, for example, hypertension (7). However, research (1) clearly suggests that all such cures must be developed with care.

AUTHOR CONTRIBUTIONS

AZ and ES conceived the work. AZ contributed data. EN and ES designed research and wrote the manuscript. EN analyzed the data and performed the research.

FUNDING

Partially supported by grants AFOSR FA9550-14-1-0060 and NSF 1817936.

SUPPLEMENTARY MATERIAL

The Supplementary Material for this article can be found online at: https://www.frontiersin.org/articles/10.3389/fimmu.2019.00004/full#supplementary-material

REFERENCES

1. Kohlhapp FJ, Huelsmann EJ, Lacek AT, Schenkel JM, Lusciks J, Broucek JR, et al. Non-oncogenic acute viral infections disrupt anti-cancer responses and lead to accelerated cancer-specific host death. *Cell Rep.* (2016) 17:957–65. doi: 10.1016/j.celrep.2016.09.068
2. Zloza A. Viruses, bacteria, and parasites - oh my! a resurgence of interest in microbial-based therapy for cancer. *J Immunother Cancer* (2018) 6:3. doi: 10.1186/s40425-017-0312-8
3. Grossman Z, Paul WE. Adaptive cellular interactions in the immune system: the tunable activation threshold and the significance of subthreshold responses. *Proc Natl Acad Sci USA* (1992) 89:10365–9. doi: 10.1073/pnas.89.21.10365
4. Grossman Z, Paul WE. Autoreactivity, dynamic tuning and selectivity. *Curr Opin Immunol.* (2001) 13:687–98. doi: 10.1016/S0952-7915(01)00280-1
5. Grossman Z, Paul WE. Dynamic tuning of lymphocytes: physiological basis, mechanisms, and function. *Annu Rev Immunol.* (2015) 33:677–713. doi: 10.1146/annurev-immunol-032712-100027
6. Alon U. *An Introduction to Systems Biology: Design Principles of Biological Circuits*. Boca Raton, FL: CRC Press (2006).
7. Dampney RA, Tan PS, Sheriff MJ, Fontes MA, Horiuchi J. Cardiovascular effects of angiotensin II in the rostral ventrolateral medulla: the push-pull hypothesis. *Curr Hypertens Rep.* (2007) 9:222–7. doi: 10.1007/s11906-007-0040-4
8. Zinselmeyer BH, Heydari S, Sacristan C, Nayak D, Cammer M, Herz J, et al. PD-1 promotes immune exhaustion by inducing antiviral T cell motility paralysis. *J Exp Med.* (2013) 210:757–74. doi: 10.1084/jem.20121416
9. Platt J. Certain systematic methods of scientific thinking may produce much more rapid progress than others. *Science (New York, NY).* (1964) 146:347–53. doi: 10.1126/science.146.3642.347
10. Marchuk GI. *Mathematical Modelling of Immune Response in Infectious Diseases*. vol. 395. Dordrecht: Springer Science & Business Media (1997).
11. Levin D, Forrest S, Banerjee S, Clay C, Cannon J, Moses M, et al. A spatial model of the efficiency of T cell search in the influenza-infected lung. *J Theor Biol.* (2016) 398:52–63. doi: 10.1016/j.jtbi.2016.02.022
12. Owen JA, Punt J, Stanford SA, Jones PP. *Kuby Immunology*. New York, NY: W.H.Freeman and Company (2013).
13. Ford WL, Gowans JL. The traffic of lymphocytes. *Semin Hematol.* (1969) 6:67–83.
14. Van den Berg H. *Mathematical Models of Biological Systems*. New York, NY: Oxford University Press (2011).
15. Poleszczuk JT, Luddy KA, Prokopiou S, Robertson-Tessi M, Moros EG, Fishman M, et al. Abscopal benefits of localized radiotherapy depend on activated T-cell trafficking and distribution between metastatic lesions. *Cancer Res.* (2016) 76:1009–18. doi: 10.1158/0008-5472.CAN-15-1423
16. Ganusov VV, Auerbach J. Mathematical modeling reveals kinetics of lymphocyte recirculation in the whole organism. *PLoS Comput Biol.* (2014) 11:e1003586. doi: 10.1371/journal.pcbi.1003586
17. Toapanta FR, Ross TM. Impaired immune responses in the lungs of aged mice following influenza infection. *Respir Res.* (2009) 10:112. doi: 10.1186/1465-9921-10-112
18. Odoardi F, Sie C, Streyl K, Ulaganathan VK, Schlager C, Lodygin D, et al. T cells become licensed in the lung to enter the central nervous system. *Nature* (2012) 488:675–9. doi: 10.1038/nature11337
19. Anderson KG, Sung H, Skon CN, Lefrancois L, Deisinger A, Vezys V, et al. Cutting edge: intravascular staining redefines lung CD8 T cell responses. *J Immunol.* (2012) 189:2702–6. doi: 10.4049/jimmunol.1201682
20. Klonowski KD, Williams KJ, Marzo AL, Blair DA, Lingenheld EG, Lefrancois L. Dynamics of blood-borne CD8 memory T cell migration *in vivo*. *Immunity* (2004) 20:551–62. doi: 10.1016/S1074-7613(04)00103-7
21. Bromley SK, Mempel TR, Luster AD. Orchestrating the orchestrators: chemokines in control of T cell traffic. *Nat Immunol.* (2008) 9:970–80. doi: 10.1038/ni.f.213
22. Alsaab HO, Sau S, Alzhrani R, Tatiparti K, Bhise K, Kashaw SK, et al. PD-1 and PD-L1 checkpoint signaling inhibition for cancer immunotherapy: mechanism, combinations, and clinical outcome. *Front Pharmacol.* (2017) 8:561. doi: 10.3389/fphar.2017.00561
23. Cheng X, Veverka V, Radhakrishnan A, Waters LC, Muskett FW, Morgan SH, et al. Structure and interactions of the human programmed cell death 1 receptor. *J Biol Chem.* (2013) 288:11771–85. doi: 10.1074/jbc.M112.448126
24. Sakaguchi S, Yamaguchi T, Nomura T, Ono M. Regulatory T cells and immune tolerance. *Cell* (2008) 133:775–87. doi: 10.1016/j.cell.2008.05.009
25. Fife BT, Pauken KE, Eagar TN, Obu T, Wu J, Tang Q, et al. Interactions between PD-1 and PD-L1 promote tolerance by blocking the

TCR-induced stop signal. *Nat Immunol.* (2009) 10:1185–92. doi: 10.1038/ni.1790
26. Francisco LM, Sage PT, Sharpe AH. The PD-1 pathway in tolerance and autoimmunity. *Immunol Rev.* (2010) 236:219–42. doi: 10.1111/j.1600-065X.2010.00923.x
27. Galante A, Tamada K, Levy D. B7-H1 and a mathematical model for cytotoxic T cell and tumor cell interaction. *Bull Math Biol.* (2012) 74:91–102. doi: 10.1007/s11538-011-9665-1
28. Schietinger A, Greenberg PD. Tolerance and exhaustion: defining mechanisms of T cell dysfunction. *Trends Immunol.* (2014) 35:51–60. doi: 10.1016/j.it.2013.10.001
29. Bardhan K, Anagnostou T, Boussiotis VA. The PD1:PD-L1/2 pathway from discovery to clinical implementation. *Front Immunol.* (2016) 7:550. doi: 10.3389/fimmu.2016.00550
30. Lu P, Youngblood BA, Austin JW, Mohammed AU, Butler R, Ahmed R, et al. Blimp-1 represses CD8 T cell expression of PD-1 using a feed-forward transcriptional circuit during acute viral infection. *J Exp Med.* (2014) 211:515–27. doi: 10.1084/jem.20130208
31. Collins MH, Henderson AJ. Transcriptional regulation and T cell exhaustion. *Curr Opin HIV AIDS* (2014) 9:459–63. doi: 10.1097/COH.0000000000000091
32. Wherry EJ, Ha SJ, Kaech SM, Haining WN, Sarkar S, Kalia V, et al. Molecular signature of CD8+ T cell exhaustion during chronic viral infection. *Immunity* (2007) 27:670–84. doi: 10.1016/j.immuni.2007.09.006
33. Martins G, Calame K. Regulation and functions of Blimp-1 in T and B lymphocytes. *Annu Rev Immunol.* (2008) 26:133–69. doi: 10.1146/annurev.immunol.26.021607.090241
34. Calame K. Activation-dependent induction of Blimp-1. *Curr Opin Immunol.* (2008) 20:259–64. doi: 10.1016/j.coi.2008.04.010
35. Sciammas R, Li Y, Warmflash A, Song Y, Dinner AR, Singh H. An incoherent regulatory network architecture that orchestrates B cell diversification in response to antigen signaling. *Mol Syst Biol.* (2011) **7**:495. doi: 10.1038/msb.2011.25
36. Singh H, Khan AA, Dinner AR. Gene regulatory networks in the immune system. *Trends Immunol.* (2014) 35:211–8. doi: 10.1016/j.it.2014.03.006
37. Daniels MA, Teixeiro E. TCR signaling in T cell memory. *Front Immunol.* (2015) 6:617. doi: 10.3389/fimmu.2015.00617
38. Speiser DE, Ho PC, Verdeil G. Regulatory circuits of T cell function in cancer. *Nat Rev Immunol.* (2016) 16:599–611. doi: 10.1038/nri.2016.80
39. Shaffer AL, Lin KI, Kuo TC, Yu X, Hurt EM, Rosenwald A, et al. Blimp-1 orchestrates plasma cell differentiation by extinguishing the mature B cell gene expression program. *Immunity* (2002) 17:51–62. doi: 10.1016/S1074-7613(02)00335-7
40. Shaffer AL, Yu X, He Y, Boldrick J, Chan EP, Staudt LM. BCL-6 represses genes that function in lymphocyte differentiation, inflammation, and cell cycle control. *Immunity* (2000) 13:199–212. doi: 10.1016/S1074-7613(00)00020-0
41. Pasqualucci L, Dominguez-Sola D, Chiarenza A, Fabbri G, Grunn A, Trifonov V, et al. Inactivating mutations of acetyltransferase genes in B-cell lymphoma. *Nature* (2011) 471:189–95. doi: 10.1038/nature09730
42. Pasqualucci L, Migliazza A, Basso K, Houldsworth J, Chaganti RS, Dalla-Favera R. Mutations of the BCL6 proto-oncogene disrupt its negative autoregulation in diffuse large B-cell lymphoma. *Blood* (2003) 101:2914–23. doi: 10.1182/blood-2002-11-3387
43. Martinez MR, Corradin A, Klein U, Alvarez MJ, Toffolo GM, di Camillo B, et al. Quantitative modeling of the terminal differentiation of B cells and mechanisms of lymphomagenesis. *Proc Natl Acad Sci USA* (2012) 109:2672–7. doi: 10.1073/pnas.1113019109
44. Sciammas R, Shaffer AL, Schatz JH, Zhao H, Staudt LM, Singh H. Graded expression of interferon regulatory factor-4 coordinates isotype switching with plasma cell differentiation. *Immunity* (2006) **25**:225–36. doi: 10.1016/j.immuni.2006.07.009
45. Shaffer AL, Emre NC, Romesser PB, Staudt LM. IRF4: immunity. malignancy! therapy? *Clin Cancer Res.* (2009) 15:2954–61. doi: 10.1158/1078-0432.CCR-08-1845
46. Man K, Miasari M, Shi W, Xin A, Henstridge DC, Preston S, et al. The transcription factor IRF4 is essential for TCR affinity-mediated metabolic programming and clonal expansion of T cells. *Nat Immunol.* (2013) **14**:1155–65. doi: 10.1038/ni.2710
47. Iwata A, Durai V, Tussiwand R, Briseno CG, Wu X, Grajales-Reyes GE, et al. Quality of TCR signaling determined by differential affinities of enhancers for the composite BATF-IRF4 transcription factor complex. *Nat Immunol.* (2017) 18:563–72. doi: 10.1038/ni.3714
48. Boddicker RL, Kip NS, Xing X, Zeng Y, Yang ZZ, Lee JH, et al. The oncogenic transcription factor IRF4 is regulated by a novel CD30/NF-κB positive feedback loop in peripheral T-cell lymphoma. *Blood* (2015) 125:3118–27. doi: 10.1182/blood-2014-05-578575
49. Vasanthakumar A, Liao Y, Teh P, Pascutti MF, Oja AE, Garnham AL, et al. The TNFReceptor superfamily-NF-κB axis is critical to maintain effector regulatory T cells in lymphoid and non-lymphoid tissues. *Cell Rep.* (2017) 20:2906–20. doi: 10.1016/j.celrep.2017.08.068
50. Ahmed A, Nandi D. T cell activation and function: role of signal strength. In: Molina-Paris C, Lyther G, editors. *Mathematical Models and Immune Cell Biology*. New York, NY; Dordrecht; Heidelberg; London: Springer (2011). p. 75–105. doi: 10.1007/978-1-4419-7725-0_4
51. Paul S, Schaefer BC. A new look at T cell receptor signaling to nuclear factor-κB. *Trends Immunol.* (2013) 34:269–81. doi: 10.1016/j.it.2013.02.002
52. Shaffer AL, Emre NC, Lamy L, Ngo VN, Wright G, Xiao W, et al. IRF4 addiction in multiple myeloma. *Nature* (2008) 454:226–31. doi: 10.1038/nature07064
53. Oreskes N, Shrader-Frechette K, Belitz K. Verification, validation, and confirmation of numerical models in the earth sciences. *Science* (1994) 263:641–6. doi: 10.1126/science.263.5147.641
54. Roshani R, McCarthy F, Hagemann T. Inflammatory cytokines in human pancreatic cancer. *Cancer Lett.* (2014) 345:157–63. doi: 10.1016/j.canlet.2013.07.014
55. Dittrich A, Hessenkemper W, Schaper F. Systems biology of IL-6, IL-12 family cytokines. *Cytokine Growth Factor Rev.* (2015) 26:595–602. doi: 10.1016/j.cytogfr.2015.07.002
56. Duvigneau S, Sharma-Chawla N, Boianelli A, Stegemann-Koniszewski S, Nguyen VK, Bruder D, et al. Hierarchical effects of pro-inflammatory cytokines on the post-influenza susceptibility to pneumococcal coinfection. *Sci Rep.* (2016) 6:37045. doi: 10.1038/srep37045
57. Minn AJ, Wherry EJ. Combination cancer therapies with immune checkpoint blockade: convergence on interferon signaling. *Cell* (2016) 165:272–5. doi: 10.1016/j.cell.2016.03.031
58. Odenthal J, Takes R, Friedl P. Plasticity of tumor cell invasion: governance by growth factors and cytokines. *Carcinogenesis* (2016) 37:1117–28. doi: 10.1093/carcin/bgw098
59. Martins GA, Cimmino L, Liao J, Magnusdottir E, Calame K. Blimp-1 directly represses Il2 and the Il2 activator Fos, attenuating T cell proliferation and survival. *J Exp Med.* (2008) 205:1959–65. doi: 10.1084/jem.20080526
60. Richards DM, Kyewski B, Feuerer M. Re-examining the nature and function of self-reactive T cells. *Trends Immunol.* (2016) 37:114–25. doi: 10.1016/j.it.2015.12.005
61. Liu Z, Ravindranathan R, Kalinski P, Guo ZS, Bartlett DL. Rational combination of oncolytic vaccinia virus and PD-L1 blockade works synergistically to enhance therapeutic efficacy. *Nat Commun.* (2017) 8:14754. doi: 10.1038/ncomms14754
62. Nirschl CJ, Drake CG. Molecular pathways: coexpression of immune checkpoint molecules: signaling pathways and implications for cancer immunotherapy. *Clin Cancer Res.* (2013) 19:4917–24. doi: 10.1158/1078-0432.CCR-12-1972
63. Stein JV, Moalli F, Ackerknecht M. Basic rules of T cell migration. In: Donnadieu E, editor. *Defects in T Cell Trafficking and Resistance to Cancer Immunotherapy* Springer (2016). p. 1–19. doi: 10.1007/978-3-319-42223-7_1
64. Lai X, Friedman A. Combination therapy of cancer with cancer vaccine and immune checkpoint inhibitors: a mathematical model. *PLoS ONE* (2017) 12:e0178479. doi: 10.1371/journal.pone.0178479
65. Nikolopoulou E, Johnson LR, Harris D, Nagy JD, Stites EC, Kuang Y. Tumour-immune dynamics with an immune checkpoint inhibitor. *Lett Biomathematics* (2018) 5:137–159. doi: 10.1080/23737867.2018.1440978
66. Pauken KE, Sammons MA, Odorizzi PM, Manne S, Godec J, Khan O, et al. Epigenetic stability of exhausted T cells limits durability of reinvigoration by PD-1 blockade. *Science* (2016) 354:1160–5. doi: 10.1126/science.aaf2807
67. Wang C, Singer M, Anderson AC. Molecular dissection of CD8(+) T-cell dysfunction. *Trends Immunol.* (2017) 38:567–76. doi: 10.1016/j.it.2017.05.008

68. Liechtenstein T, Dufait I, Bricogne C, Lanna A, Pen J, Breckpot K, et al. PD-L1/PD-1 co-stimulation, a brake for T cell activation and a T cell differentiation signal. *J Clin Cell Immunol.* (2012) S12:006. doi: 10.4172/2155-9899.S12-006
69. Siefker-Radtke A, Curti B. Immunotherapy in metastatic urothelial carcinoma: focus on immune checkpoint inhibition. *Nat Rev Urol.* (2018) 15:112–24. doi: 10.1038/nrurol.2017.190
70. Kumar A, Takada Y, Boriek AM, Aggarwal BB. Nuclear factor-κB: its role in health and disease. *J Mol Med*. (2004) 82:434–48. doi: 10.1007/s00109-004-0555-y
71. Liu T, Zhang L, Joo D, Sun SC. NF-κB signaling in inflammation. *Signal Transduct Target Ther.* (2017) 2:17023. doi: 10.1038/sigtrans.2017.23
72. Sun SC. The non-canonical NF-κB pathway in immunity and inflammation. *Nat Rev Immunol.* (2017) 17:545–58. doi: 10.1038/nri.2017.52
73. Westermann J, Ehlers EM, Exton MS, Kaiser M, Bode U. Migration of naive, effector and memory T cells: implications for the regulation of immune responses. *Immunol Rev*. (2001) 184:20–37. doi: 10.1034/j.1600-065x.2001.1840103.x
74. Lever M, Lim HS, Kruger P, Nguyen J, Trendel N, Abu-Shah E, et al. Architecture of a minimal signaling pathway explains the T-cell response to a 1 million-fold variation in antigen affinity and dose. *Proc Natl Acad Sci USA* (2016) 113:E6630–8. doi: 10.1073/pnas.1608820113
75. Rendall AD, Sontag ED. Multiple steady states and the form of response functions to antigen in a model for the initiation of T-cell activation. *R Soc Open Sci.* (2017) 4:170821. doi: 10.1098/rsos.170821
76. Khibnik AI, Kuznetsov YA, Levitin VV, Nikolaev EV. Continuation techniques and interactive software for bifurcation analysis of ODEs and iterated maps. *Physica D* (1993) 62:360–71. doi: 10.1016/0167-2789(93)90294-B
77. Kim D, Kwon YK, Cho KH. The biphasic behavior of incoherent feed-forward loops in biomolecular regulatory networks. *Bioessays* (2008) 30:1204–11. doi: 10.1002/bies.20839
78. Shoval O, Alon U, Sontag E. Symmetry invariance for adapting biological systems. *SIAM J Appl Dyn Syst*. (2011) 10:857–86. doi: 10.1137/100818078
79. Chiang AW, Liu WC, Charusanti P, Hwang MJ. Understanding system dynamics of an adaptive enzyme network from globally profiled kinetic parameters. *BMC Syst Biol.* (2014) 8:4. doi: 10.1186/1752-0509-8-4
80. Skataric M, Nikolaev EV, Sontag ED. Fundamental limitation of the instantaneous approximation in fold-change detection models. *IET Syst Biol.* (2015) 9:1–15. doi: 10.1049/iet-syb.2014.0006
81. Sontag ED. A dynamic model of immune responses to antigen presentation predicts different regions of tumor or pathogen elimination. *Cell Syst*. (2017) 4:1–11. doi: 10.1016/j.cels.2016.12.003
82. Rahman A, Tiwari A, Narula J, Hickling T. Importance of feedback and feedforward loops to adaptive immune response modeling. *CPT Pharmacometrics Syst Pharmacol.* (2018) 7:621–8. doi: 10.1002/psp4.12352
83. Wu J, Shi X, Xiao X, Minze L, Wang J, Ghobrial RM, et al. IRF4 controls a core regulatory circuit of T cell dysfunction in transplantation. *J Immunol.* (2017) 198(1 Suppl.):124.10.
84. Wu J, Zhang H, Shi X, Xiao X, Fan Y, Minze LJ, et al. Ablation of transcription factor IRF4 promotes transplant acceptance by driving allogenic CD4+ T cell dysfunction. *Immunity* (2017) 47:1114–28.e6. doi: 10.1016/j.immuni.2017.11.003
85. Chennupati V, Held W. Feeling exhausted? Tuning Irf4 energizes dysfunctional T cells. *Immunity* (2017) 47:1009–11. doi: 10.1016/j.immuni.2017.11.028
86. Štefanová I, Hemmer B, Vergelli M, Martin R, Biddison WE, Germain RN. TCR ligand discrimination is enforced by competing ERK positive and SHP-1 negative feedback pathways. *Nat Immunol.* (2003) 4:248–54. doi: 10.1038/ni895
87. François P, Voisinne G, Siggia ED, Altan-Bonnet G, Vergassola M. Phenotypic model for early T-cell activation displaying sensitivity, specificity, and antagonism. *Proc Natl Acad Sci USA* (2013) 110:E888–897. doi: 10.1073/pnas.1300752110
88. Watson HA, Wehenkel S, Matthews J, Ager A. SHP-1: the next checkpoint target for cancer immunotherapy? *Biochem Soc Trans.* (2016) 44:356–62. doi: 10.1042/BST20150251
89. Ohaegbulam KC, Assal A, Lazar-Molnar E, Yao Y, Zang X. Human cancer immunotherapy with antibodies to the PD-1 and PD-L1 pathway. *Trends Mol Med*. (2015) 21:24–33. doi: 10.1016/j.molmed.2014.10.009
90. Arasanz H, Gato-Canas M, Zuazo M, Ibanez-Vea M, Breckpot K, Kochan G, et al. PD1 signal transduction pathways in T cells. *Oncotarget* (2017) 8:51936–45. doi: 10.18632/oncotarget.17232
91. Kuznetsov VA, Makalkin IA, Taylor MA, Perelson AS. Nonlinear dynamics of immunogenic tumors: parameter estimation and global bifurcation analysis. *Bull Math Biol.* (1994) 56:295–321. doi: 10.1007/BF02460644
92. Bocharov G, Volpert V, Ludewig B, Meyerhans A. *Mathematical Immunology of Virus Infections*, Vol. 4. Cham: Springer (2018).
93. Grebennikov D, Bocharov G. Modelling the structural organization of lymph nodes. In: *Evolutionary Computation (CEC), 2017 IEEE Congress on*. Red Hook, NY: IEEE (2017). p. 2653–5.
94. Tretyakova RM, Lobov GI, Bocharov GA. Modelling lymph flow in the lymphatic system: from 0D to 1D spatial resolution. *Math Model Nat Phenomena* (2018) 13:45. doi: 10.1051/mmnp/2018044
95. McNamara HA, Cai Y, Wagle MV, Sontani Y, Roots CM, Miosge LA, et al. Up-regulation of LFA-1 allows liver-resident memory T cells to patrol and remain in the hepatic sinusoids. *Sci Immunol.* (2017) 2:eaaj1996. doi: 10.1126/sciimmunol.aaj1996
96. Bocharov G, Romanyukha A. Mathematical model of antiviral immune response III. Influenza A virus infection. *J Theor Biol*. (1994) 167:323–60. doi: 10.1006/jtbi.1994.1074
97. Smith AM, Perelson AS. Influenza A virus infection kinetics: quantitative data and models. *Wiley Interdiscipl Rev Syst Biol Med*. (2011) 3:429–45. doi: 10.1002/wsbm.129
98. Lipniacki T, Hat B, Faeder JR, Hlavacek WS. Stochastic effects and bistability in T cell receptor signaling. *J Theor Biol.* (2008) 254:110–22. doi: 10.1016/j.jtbi.2008.05.001
99. Horsfall FL. Reproduction of influenza viruses; quantitative investigations with particle enumeration procedures on the dynamics of influenza A and B virus reproduction. *J Exp Med.* (1955) 102:441–73. doi: 10.1084/jem.102.4.441
100. Bertalanffy FD, McAskill C. Rate of cell division of malignant mouse melanoma B16. *J Natl Cancer Inst.* (1964) 32:535–44.
101. Carlson JA. Tumor doubling time of cutaneous melanoma and its metastasis. *Am J Dermatopathol.* (2003) 25:291–9. doi: 10.1097/00000372-200308000-00003
102. Radunskaya A, Kim R, Woods I, et al. Mathematical modeling of tumor immune interactions: a closer look at the role of a PD-L1 inhibitor in cancer immunotherapy. *Spora* (2018) 4:25–41. doi: 10.30707/SPORA4.1Radunskaya
103. Kosinsky Y, Dovedi SJ, Peskov K, Voronova V, Chu L, Tomkinson H, et al. Radiation and PD-(L)1 treatment combinations: immune response and dose optimization via a predictive systems model. *J Immunother Cancer* (2018) 6:17. doi: 10.1186/s40425-018-0327-9
104. Kaufman HL, Kohlhapp FJ, Zloza A. Oncolytic viruses: a new class of immunotherapy drugs. *Nat Rev Drug Discov*. (2015) 14:642–62. doi: 10.1038/nrd4663
105. Jhawar SR, Thandoni A, Bommareddy PK, Hassan S, Kohlhapp FJ, Goyal S, et al. Oncolytic viruses-natural and genetically engineered cancer immunotherapies. *Front Oncol.* (2017) 7:202. doi: 10.3389/fonc.2017.00202
106. Samson A, Scott KJ, Taggart D, West EJ, Wilson E, Nuovo GJ, et al. Intravenous delivery of oncolytic reovirus to brain tumor patients immunologically primes for subsequent checkpoint blockade. *Sci Transl Med.* (2018) 10:eaam7577. doi: 10.1126/scitranslmed.aam7577

Conflict of Interest Statement: The authors declare that the research was conducted in the absence of any commercial or financial relationships that could be construed as a potential conflict of interest.

frontiers

Supplementary Material

Immunobiochemical Reconstruction of Influenza Lung Infection - Melanoma Skin Cancer Interactions

SI-1 A REVIEW OF RELEVANT LITERATURE

SI-1.1 An immunobiochemical reconstruction scope

Given the complexity of the processes relevant to the observations **(O1)** - **(O5)**, we must limit the scope of our research. Because the interaction between PD-1 and PD-L1 is regarded as a major "T cell brake" (Nirschl and Drake, 2013), and because it is also a central topic in (Kohlhapp et al., 2016), we center our analysis on the construction of the gene regulatory networks (GRNs) directly involved in the expression of PD-1 receptors under different immunologic contexts.

A very important topic that shapes the scope of our work is that T cell activities are controlled at multiple levels. These regulatory controls are necessary to prevent T cells from becoming hyperactivated, causing significant collateral damage to non-target tissue. These types of responses enhance inflammation, resulting in the release of self-antigens from necrotic tissue, increasing the chances for the induction of autoimmune diseases (Liechtenstein et al., 2012). To avoid autoimmunity induced by necrotic tissue, key regulatory T cell inhibitory interactions occur between PD-L1 expressed on immune, infected and tumor cells (Nirschl and Drake, 2013), and, PD-1 expressed on T cells (Sakaguchi et al., 2008; Fife et al., 2009; Francisco et al., 2010; Nirschl and Drake, 2013; Schietinger and Greenberg, 2014; Bardhan et al., 2016; Sharpe and Pauken, 2017).

SI-1.2 A TCR activation primer

For a strong CD8+ T cell activation, three well-known signals have to be provided from professional antigen presenting cells (APCs) (Kindt et al., 2007):

- Signal 1: Antigen presentation to T cells.
- Signal 2: Co-stimulation.
- Signal 3: Cytokine priming.

Signal 1 is mediated by binding of a T cell receptor (TCR) on T cells with its cognate antigen presented on an MHC.

Signal 2 is mediated by a series of receptor:ligand bindings, such as CD80 binding to CD28 between the APC and the T cell, respectively. The combination of TCR engagement, CD28 binding, and IL-2 activates Zap-70, lck and PI3K, which in turn lead to T cell activation, expansion, and acquisition of effector activities (Liechtenstein et al., 2012; Rendall and Sontag, 2017). Furthermore, in reality, as Liechtenstein et al. (2012) states, a variety of ligand-receptor interactions take place in the immunological synapse, many of which are inhibitory. The final integration between activatory and inhibitory interactions determine the type and strength of the co-stimulatory signal given to the T cells, setting the "degree" of T cell activation.

Signal 3 is mediated by binding of cytokines to their respective receptors, such as IL-2 produced by T cells binding to IL-2 receptors also on the same T cells.

During antigen presentation to naïve T cells, PD-1:PD-L1 interaction acts as a brake in TCR signal transduction (Nirschl and Drake, 2013). PD-1 is transiently up-regulated during antigen presentation as a consequence of T cell activation (Freeman et al., 2000) and PD-1:PD-L1 binding results in ligand-induced TCR down-modulation (Escors et al., 2011; Karwacz et al., 2011, 2012).

To this end, Liechtenstein et al. (2012) suggest that TCR down-modulation is absolutely required for T cell activation in order to prevent T cell hyperactivation by terminating TCR signal transduction. In such cases, PD-1 associates to the TCR at the immunological synapse and controls its signal transduction as well

as its presence on the T cell surface (Karwacz et al., 2011). TCR down-modulation is largely reduced when PD-L1 is silenced in antigen-presenting DCs, or when PD-1:PD-L1 is blocked using antibodies during antigen presentation (Liechtenstein et al., 2012).

Finally, as further reviewed in (Liechtenstein et al., 2012), PD-1:PD-L1 interactions control the timing of TCR stimulation in at least two different ways: (*i*) by removing TCRs from the T cell surface, and (*ii*) by terminating the intracellular signal transduction pathways after recruiting phosphatases SHP1 and SHP2 (Zhang and Rundell, 2006; Bardhan et al., 2016). Note briefly that processes in (*ii*), put, for example, a brake on NF-κB signaling, the inhibitory process that shuts down IRF4, which in turn removes the Blimp-1 imposed brake from PD-1 transcription, where both IRF4 and Blimp-1 are key molecular species of our analysis, as discussed below in detail.

SI-1.3 Linking observations with immunological mechanisms

(O1) Anti-tumor CD8+ T cells are shunted to the lung during influenza infection.

Here, we discuss six mechanisms (O1-M1) - (O1-M6). In order to get insight into mechanism (O1-M1), we subdivide mechanism (O1-M1-B) into two complementary immunological mechanisms (O1-M1-A) and (O1-M1-B).

Mechanism (O1-M1-A) Cytotoxic CD8+ T cells ($\mathrm{T_{EFF}}$) are highly dynamic within dense tissue once activated, immediately followed by their migration arrest, induced by integrin upregulation that stops motion and promotes effective synapse formation (Feinerman et al., 2008) when contacting a high potency antigen available at adequate density on tissue resident antigen-presenting cells (APCs) (Marelli-Berg et al., 2010; Honda et al., 2014). Indeed, T cells in tissues migrate along chemotactic gradients until they encounter antigen on an APC, which leads to their Intercellular Adhesion Molecule (ICAM-1)-dependent arrest by TCR-mediated "stop signals" (Jennrich et al., 2012).

Specifically, activated T cells have been shown to rapidly traffic in tissue in response to chemokines and cytokines (Kindt et al., 2007; Chimen et al., 2017), including CXCL9, CXCL10, INFγ, *etc.* (Ogawa et al., 2002; Baaten et al., 2013; Oelkrug and Ramage, 2014; Kim and Chen, 2016; Spranger, 2016; Stein et al., 2016) with a primary function to find and kill target cells expressing cognate antigen (Ag) (Bhat et al., 2014).

Dynamic speed and travel patterns of $\mathrm{T_{EFF}}$ are predominantly influenced by the tissue environment rather than by mechanisms intrinsic to the $\mathrm{T_{EFF}}$. Specifically, activated T cells have been shown *in vivo* to traffic to inflamed skin, even in the absence of cognate Ag (Biotec and Gladbach, 2011), suggesting that Ag alone does not play an essential role in the recruitment of circulating CD8+ T cells (Van Braeckel-Budimir and Harty, 2017).

To this end, a natural question arises: "Why is it the anti-tumor $\mathrm{T_{EFF}}$ cells that are shunted to the infected lung, and not vice versa, that is, why is it not the anti-influenza $\mathrm{T_{EFF}}$ cells that are shunted to the tumor compartment instead?"

Mechanism (O1-M1-B) The above question can be addressed by reviewing *in vivo* studies describing T cell *Ag-induced arrest* in tissues in direct proportion to the amount of Ag present (Beattie et al., 2010; Deguine et al., 2010; Celli et al., 2011; Honda et al., 2014). Indeed, the time needed for the $\mathrm{T_{EFF}}$ killing of highly antigenic cells *in vivo* through the cell-to-cell attachment and TCR-pMHC (Ag) binding events can be partiality attributed to effective half-life or "confinement time" of a TCR-pMHC interaction (Aleksic et al., 2010).

The process can last for long periods of time depending on the context, (*i*) in the range of 40 minutes, (*ii*) over 3-6 hours and (*iii*) up to 48 hours, in order to form "stable immunologic synapses" (Grakoui et al., 1999; Liechtenstein et al., 2012; Xie et al., 2013; Tkach and Altan-Bonnet, 2013; Ortega-Carrion and Vicente-Manzanares, 2016; Stein et al., 2016), which are needed to complete a series of signaling events, including co-receptor recruitment and TCR phosphorylation (McKeithan, 1995; Garcia et al., 2007; Breart et al., 2008; Tkach and Altan-Bonnet, 2013; Liu et al., 2014; Das et al., 2015; Parello and Huseby, 2015).

Although T cells become rapidly arrested after their contact with Ag-presenting tissue-resident cells, their subsequent recovery period was found to be heterogeneous, with some cells regaining motility within 30 min and others remaining arrested for several hours (Honda et al., 2014). After the extended arrest, T cells can be oscillating between periods of brief arrest and motility, suggestive of additional TCR stimulation, before regaining a migration pattern similar to what was observed in the absence of antigen (Honda et al., 2014).

Such Ag-induced arrested T cells are functionally very distinct of highly motile T cells, because the arrested T cells were found to be characterized by a profoundly increased production of INFγ (Honda et al., 2014).

All this suggests that T cell Ag-induced arrest on target cells positively correlates with their effector function, and the balance between motility and Ag-induced arrest controls T cell activation (Stein et al., 2016).

Here, the definitions of "long periods of time" and "stable immunologic synapses" should be understood dynamically and not statically in terms of "fast association and dissociation rates" (Coombs et al., 2011; Tkach and Altan-Bonnet, 2013) that define the "confinement time" of a TCR-pMHC interaction (Aleksic et al., 2010). Multiple studies have indicated that T cells integrate these discontinuous antigen contacts over time and respond in proportion to the cumulative duration of TCR signaling as reviewed in (Tkach and Altan-Bonnet, 2013).

Many tumor-specific antigens provoke only weak immune responses, which are incapable of eliminating all tumor cells (Aleksic et al., 2010). This is in line with the McKeithan-Altan-Bonnet-Germain kinetic proofreading model (KPL-IFFL) (Hopfield, 1974; McKeithan, 1995; Altan-Bonnet and Germain, 2005; François et al., 2013; Courtney et al., 2017), which is based on the well-established fact that T cell activation is selected by evolution to discriminate a few foreign peptides rapidly from a vast excess of self-peptides (François et al., 2013). We use the abbreviation KPL-IFFL for the kinetic proofreading model coupled with limited signaling and incoherent feedforward loop (Lever et al., 2016).

Because many tumor antigens are self antigens (Liechtenstein et al., 2012), often called Tumour-Associated Antigens (TAAs) and Tumor-Specific Antigens (TSA) (Kindt et al., 2007), anti-tumor TCRs may be of lower affinity due to their selection and training against "self"-antigen reactivity (Hogquist and Jameson, 2014) compared with those TCRs evolved to recognize viral epitopes (Irving et al., 2012; Vonderheide and June, 2014). Indeed, the affinity of TCR clones for novel or not previously encountered antigens, like tumor antigens, is remarkably low, typically 1 - 10 μM (Courtney et al., 2017). This is in line with a commonly accepted fact that high-affinity tumour-specific TCR clonotypes are typically deleted from the available repertoire during thymic selection because the vast majority of targeted epitopes are derived from autologous proteins (Tan et al., 2015).

This phenomenon is known as "antigen discrimination" (Galvez et al., 2016; Rendall and Sontag, 2017), and is currently discussed in terms of the "antigen-receptor (catch bonds) lifetime dogma" (Feinerman et al., 2008; François and Altan-Bonnet, 2016).

In addition to the TCR antigen discrimination, tumors do not express large amounts of cognate Ag on MHCs to keep systemic tolerance and prevent the development of autoimmune diseases (Liechtenstein et al., 2012; Nirschl and Drake, 2013), compared with viral infection.

Antigen expression by tumor cells thus determines $\mathrm{T_{EFF}}$ motility within the tumor (Boissonnas et al., 2007). Such mobile $\mathrm{T_{EFF}}$ cells can follow collagen fibers or blood vessels, or migrate along blood vessels preferentially adopting an elongated morphology (Boissonnas et al., 2007), when nothing can prevent them from freely moving along high infection-induced chemokine gradients toward the infected and inflamed lung.

We finalize the description of this mechanism by pointing out a very important and relevant study (Poleszczuk et al., 2016) which documents intensive motility of anti-timor $\mathrm{T_{EFF}}$ cells when the anti-timor $\mathrm{T_{EFF}}$ cells enter and leave the TME back to the bloodstream and lymph multiple times before they get finally arrested and absorbed by the multiple-time revisited TME.

Mechanism (O1-M2) Tumors themselves may induce emigration of tumor-specific CD8+ T cells from the TME by employing chemokines like SDF-1/CXCL12 (Marelli-Berg et al., 2010; Joyce and Fearon, 2015; Kim and Chen, 2016). When the level of CXCL12 becomes greater than the levels of other chemoattractors, CXCL12 acts as chemorepeller (Marelli-Berg et al., 2010; Vianello et al., 2005), that is, at low levels, CXCL12 is a chemoattractor, while at high levels CXCL12 is a chemorepeller. Expression of CXCL12 and its receptor CXCR4 is induced by IFNγ (Ogawa et al., 2002; de Oliveira et al., 2013).

Sometimes, this effect is called *fugetaxis* (Vianello et al., 2005). Because IFNγ is produced in large quantities by different cell types in inflamed infected sites (Kindt et al., 2007), and then circulates to the tumor site within the bloodstream, it can be concluded that (distant) infection can significantly contribute to the egress of anti-tumor CD8+ T cells from the TME.

Mechanism (O1-M3) Due to non-specific cardiovascular edema effects, caused by infection-induced inflammation (Marchuk, 1997), the general circulation pattern of central memory ($\mathrm{T_{CM}}$) and naïve T cells (Donnadieu, 2016; Levin et al., 2016) throughout the body from blood, across high endothelial venules (HEVs) into lymph nodes, through T cell zones, out via efferent lymphatics, and eventually back into the blood through the thoracic duct is significantly perturbed and is redirected to the site of infection-induced inflammation (Marchuk, 1997; Levin et al., 2016).

Mechanism (O1-M4) As mentioned earlier, different cells in infected tissues induce cytokine production (Kindt et al., 2007). Cytokines play multiple roles such as chemoattraction of dendritic cells, macrophages, T cells, NK cells, and promotion of T cell adhesion to endothelial cells (Dufour et al., 2002). To this end, significant levels of both activated influenza-specific and non-specific T cells were found present in infected lung and measured (Toapanta and Ross, 2009).

The inflammatory chemokine receptor CXCR3 has been recently identified with effective T cell function. CXCR3 expression is increased during T cell activation and is important for homing to inflammatory sites. Its ligands CXCL9, CXCL10 and CXCL11 are rapidly induced during inflammation and guide T cells into specific microenvironments in lymphoid and non-lymphoid tissues as reviewed in (Stein et al., 2016).

Mechanism (O1-M5) High levels of IL-2 produced by activated anti-infection CD8+ T cells at the infection site counteract the repelling action of CXCL12 (Beider et al., 2003) in contrast to the opposite effect elicited by CXCL12 in the TME as discussed earlier.

Mechanism (O1-M6) The PD-1 mediated control of immune responses depends on interactions between PD-1 on CD8+ T cells and PD-L1 in tissues (Nirschl and Drake, 2013), inducing CD8+ T cell motility

paralysis via PD-1:PD-L1 stable bonds (Zinselmeyer et al., 2013; Schietinger and Greenberg, 2014; Stein et al., 2016). We introduce the "paralysis" mechanism **(O1-M6)** into the context of our studies by discussing systematically the following specific questions,

(Q.1) "What triggers expression of PD-1 receptors on CD8+ T cells, and why is the expression triggered in the first place?"

(Q.2) "Why are PD-1 receptors over-expressed in larger quantities on anti-tumor CD8+ T cells and not on anti-influenza CD8+ T cells co-localized within the same infected lung?"

(Q.3) "Why are anti-VACV CD8+ T cells not sequestered in the infected lung when the host is distantly co-infected with both infections, influenza A and VACV infections (in the absence of tumors)?"

To address (Q.1), we follow Simon and Labarriere (2017) who reviewed results highlighting the ambiguous role of PD-1 in defining efficient or inefficient adaptive immune response. Initially, PD-1 transient expression on native T cells is induced immediately upon TCR activation, that is, the number of PD-1 receptors can be regarded as a biomarker of activated and *not* exhausted CD8+ T cells.

The level of PD-1 receptors decreases in the absence of TCR signaling but is maintained upon chronic activation with a persistent epitope target such as in chronic viral infections and in cancer (Wherry et al., 2007; Brown et al., 2010; Pauken and Wherry, 2015b,a). Thus, the number of PD-1 receptors can *also* be regarded as a biomarker of exhausted T cells (Simon and Labarriere, 2017). Importantly, transient expressions of PD-1 and PD-L1 is viewed as a window of opportunity in the combined radiation (RT) and anti-PD-1:PD-L1 therapies (Kosinsky et al., 2018).

The discussed ambiguous role of PD-1, which can be viewed either as a biomarker of activated or exhausted CD8+ T cells depending on the inflammation context, can be explained as follows.

First, although the central immune tolerance mechanism results in the removal of most of the auto- or self-reactive T cells during thymic selection, a fraction of self-reactive lymphocytes escapes to the periphery and poses the threat of autoimmunity. Moreover, "it is now understood that the T cell repertoire is in fact broadly self-reactive, even self-centered" (Hogquist and Jameson, 2014; Grossman and Paul, 2015; Richards et al., 2016).The strength with which a T cell reacts to self ligands and the environmental context in which this reaction occurs influence almost every aspect of T cell biology, from development to differentiation to effector function (Hogquist and Jameson, 2014; Grossman and Paul, 2015).

The immune system has evolved various mechanisms to constrain autoreactive T cells and maintain peripheral tolerance (Grossman and Paul, 2001, 2015), including the constitutive expression of PD-L1 in large quantities in various tissues (*e.g.*, lungs, pancreatic islets, *etc.*), and T cell anergy, deletion, and suppression by regulatory T cells (Sakaguchi et al., 2008; Fife et al., 2009; Francisco et al., 2010; Schietinger and Greenberg, 2014; Bardhan et al., 2016).

Second, although T cells endow their host with a defense that favors pathogen clearance, this efficiency sometimes gives rise to intolerable immunopathology, especially when a pathogen transitions into a state of persistence. For this reason, the immune system is equipped with dampening mechanisms that induce T cell exhaustion via PD-1 and PD-L1 immune regulators (Zinselmeyer et al., 2013; Pauken and Wherry, 2015b; Bardhan et al., 2016). This means that the activated T cells must be attenuated irrespective of whether invaders are eliminated or persist. This is because, quite often, persisting microorganisms may cause less tissue damage than the associated immunopathology as a result of continued lymphocyte cytotoxicity (Speiser et al., 2016).

Overall, this means that the immune system prefers to put infection that cannot be eradicated rapidly into a chronic state which should produce less damage to the body than the extended exposition of the body to aggressive CD8+ T cell response (Grossman and Paul, 1992, 2015).

(O2) Disruption of anti-tumor responses is not due to tumor-induced immune suppression of viral clearance or the inability of the immune system to respond to concomitant challenges.

The observation (Kohlhapp et al., 2016) that cancer does not significantly suppress the natural anti-viral response can be explained by similar arguments used to introduce the mechanisms **(O1-M1)** - **(O1-M6)**. These suggest that much weaker inflammation in the tumor site compared with much stronger inflammation in the infected lung may not be enough to force the anti-influenza CD8+ T cells (arrested in the lung as discussed earlier) to egress the lung. The observation (Kohlhapp et al., 2016) that influenza infection did not alter the natural clearance of the VACV or the proportion of VACV-tetramer+ CD8+ T cells at the site of influenza infection can also be explained by the local anti-VACV CD8+ T cells Ag-induced arrest required to kill VACV-infected cells as discussed earlier.

(O3) Therapeutic blockade of PD-1 results in reversal of infection-mediated anti-tumor response disruption.

Recall that PD-L1 promotes motility paralysis (Zinselmeyer et al., 2013; Schietinger and Greenberg, 2014; Stein et al., 2016). In other words, the bond PD-1:PD-L1 mediates locking T cells into a state of prolonged motility paralysis by localizing to the environment with abundant PD-L1 expression on stromal cells as discussed earlier, termed "T cell motility paralysis" in (Zinselmeyer et al., 2013; Schietinger and Greenberg, 2014).

Because the bond PD-1:PD-L1 is formed dynamically due to interchanging binding and unbinding processes, blockade of PD-1 shifts the dynamic equilibrium towards dissociation of PD-1:PD-L1 bond, leading to the rapid recovering (about 30 min.) of T cell motility, signaling, and cytokine production (Zinselmeyer et al., 2013; Oelkrug and Ramage, 2014; Pauken et al., 2016). The corresponding details are summarized in Table SI-1.1 of Sect. SI-1.4.

Reactivated anti-tumor CD8+ T cells then detach from local PD-L1 anchors and start moving with lymph outside of the infected lung and may ultimately return back to the tumor site (Calzascia et al., 2005) with the blood flow, following similar trafficking routes and mechanisms as discussed in (Poleszczuk et al., 2016).

SI-1.4 Reactivation of exhausted effector cells

Because the PD-1 blockade reactivates exhausted anti-tumor CD8+ T cells, sequestered in the infected lung and return, possibly, them back to the TME (Kohlhapp et al., 2016), we briefly summarize relevant known results on the exhausted T cell reactivation (Table SI-1.1). Our summary is based on the recent reports (Zinselmeyer et al., 2013; Pauken et al., 2016; Wang et al., 2017).

Several gene signatures based on the analyses of populations of dysfunctional CD8+ T cells from cancer and chronic viral infections have been published and reviewed by Wang et al. (2017). These signatures confirm great similarity between virus- and cancer-associated CD8+ T cell dysfunction. Due to these published gene signature comparisons, we believe that Table SI-1.1 further supports mechanisms formulated in the main text.

Table SI-1.1. A brief summary of T_{EX} reactivation after PD-1 blockade.

Reactivation Effect	**Mechanisms**
(E.1) reactivation of T_{EFF} functions in T_{EX}:	
(E.1.1) *improved cell cycle and proliferation*	• increased transcription of cell division genes • increased levels of Ki-67
(E.1.2) *improved response to antigen*	• elevated co-production of INFγ and TNFα
(E.1.3) *improved motility and chemotaxis*	• upregulated expression of *cxcl9* and *cxcr3*
(E.1.4) *improved killing capability*	• increased levels of granulocytes
(E.1.5) *suppression of PD-1 expression*	• upregulated expression of *prdm1* encoding Blimp-1
(E.1.6) *protection against exhaustion*	• upregulated expression of *il7r* • OCR state specific regulation of *ctla4*
(E.2) reactivation of T_{MEM} functions in T_{EX}:	
(E.2.1) *negative regulation of apoptosis*	• increased levels of phospho-STAT5
(E.2.2) *improved adhesion*	• unknown
(E.2.3) *improved regulation of activation*	• elevated production of INFγ
(E.3) transient reinvigoration of T_{EX} (peaked in 3-weeks)	
transient and Ag-dose dependent expression of prdm1 encoding Blimp-1	• small and large amounts of Ag repress *prdm1* • medium amounts of Ag activate *prdm1*
(E.4) signaling and immunometabolic effects:	
(E.4.1) *signaling*	• upregulation of genes encoding NF-κB and IRFs
(E.4.2) *lipid metabolism*	• upregulation of genes encoding PPARγ and RXRα • downregulation of *srebp1*
(E.4.3) *de-novo cholesterol pathway, and glycolysis*	• unknown

SI-2 A CORE MATHEMATICAL MODEL OF PD-1 EXPRESSION

SI-2.1 The model equations

Our core mathematical model of PD-1 expression on the surface of a CD8+ T cell describes normal and aberrant dynamics of interactions between four immunobiochemical entities, Bcl-6 (C), PD-1 (P), IRF4 (I), and Blimp-1 (B),

$$\underbrace{\frac{dC}{dt}}_{C=[\text{Bcl6}]} = \underbrace{\left(\frac{a_c U^{n_c}}{A_c^{n_c} + U^{n_c}}\right)}_{\text{TCR dep. act.}} \underbrace{\left(\frac{M_c^{r_c}}{M_c^{r_c} + B^{r_c} + I^{r_c} + C^{r_c}}\right)}_{\text{Blimp1/IRF4/Bcl6 dep. repr.}} - \underbrace{\mu_c C,}_{\text{Bcl6 deg.}} \tag{SI-2.1a}$$

$$\underbrace{\frac{dP}{dt}}_{P=[\text{PD1}]} = \left(\sigma_p + \underbrace{\frac{a_p U^{n_p}}{A_p^{n_p} + U^{n_p}}}_{\text{TCR dep. act.}}\right) \underbrace{\left(\frac{M_p^{r_p}}{M_p^{r_p} + B^{r_p}}\right)}_{\text{Blimp1 dep. repr.}} - \underbrace{\mu_p P,}_{\text{PD1 deg.}} \tag{SI-2.1b}$$

$$\underbrace{\frac{dI}{dt}}_{I=[\text{IRF4}]} = \left(\sigma_i + \underbrace{\frac{a_i U^{n_i}}{A_i^{n_i} + U^{n_i}}}_{\text{TCR dep. act.}} + \underbrace{\frac{k_i B^{m_i}}{K_i^{m_i} + B^{m_i}}}_{\text{Blimp1 dep. act.}} + \underbrace{\frac{q_i I^{s_i}}{Q_i^{s_i} + I^{s_i}}}_{\text{IRF4 dep. act.}}\right) \Phi_{\text{L}} - \underbrace{\mu_i I,}_{\text{IRF4 deg.}} \tag{SI-2.1c}$$

$$\underbrace{\frac{dB}{dt}}_{B=[\text{Blimp1}]} = \left(\underbrace{\frac{a_b U^{n_b}}{A_b^{n_b} + U^{n_b}}}_{\text{TCR dep. act.}} + \underbrace{\frac{k_b I^{m_b}}{K_b^{m_b} + I^{m_b}}}_{\text{IRF4 dep. act.}}\right) \underbrace{\left(\frac{M_b^{r_b}}{M_b^{r_b} + C^{r_b}}\right)}_{\text{Bcl6 dep. repr.}} - \underbrace{\mu_b B.}_{\text{Blimp1 deg.}} \tag{SI-2.1d}$$

Here, for the sake of compactness in the equation term explanation, we use the following abbreviations, "TCR dep. act." for TCR-dependent activation, "Blimp-1/IRF4/Bcl-6" for Blimp-1/IRF4/Bcl-6-dependent repression, and so on.

The model structure corresponds to the circuit topology depicted in Fig. 2 of the main text with a few simplifications resulting from lumping some species, (*i*) NFATc1 and PD-1 becoming the species P, and (*ii*) NF-$\varkappa$B and IRF4 becoming the species I. We also omit Erk-dependent degradation of Bcl-6 because it is in turn attenuated by Bcl-6 itself.

The input $U := U(\alpha, \kappa, P)$ to the model (SI-2.1) is described by the scalar function $u(\alpha, \kappa)$ defined in (SI-3.11),

$$U(\alpha, \kappa, P) = u(\alpha, \kappa)\, \phi_L(P), \tag{SI-2.2a}$$

$$\phi_L(P) = \frac{H_p}{H_p + L\,P}. \tag{SI-2.2b}$$

Here, the inhibitory regulatory factor $\phi_L(P)$ corresponds to the co-localization of PD-1:PD-L1 complexes around the immunologic Ag-TCR synapses that hinder the TCR activity as discussed in Sec. SI-1.2. An external environment parameter L models a fraction of PD-1 receptors bound with PD-L1. Parameters α and κ are scaled Ag level and scaled k_{off}, the dissociation constant for the Ag-TLR bond, respectively.

We use a Michaelis-Menton saturation functional dependence in the expression (SI-2.2b) to describe a 2D-sliding diffusion of PD-1 receptors on the surface of a T cell (without any switch-like reaction sharp transitions) as a major process contributing to the TCR down regulation effect (Sect. SI-1.2).

Next, the factor $\Phi_{\rm L} := \Phi_{\rm L}(P)$ in the equation (SI-2.1c) describes a net negative feedback effect caused by the PD-1:PD-L1 interaction (Sec. SI-1.2),

$$\Phi_{\rm L}(P) \,=\, \frac{H_L^{h_L}}{H_L^{h_L} \,+\, (L\,P)^{h_L}}. \tag{SI-2.3}$$

Recall that the active complex formed between PD-1 and PD-L1 suppresses the NF-κB pathway, while the NF-κB pathway activates IRF4 (Fig. 2).

We also use generic Hill functions in (SI-2.2b) and (SI-2.3) following the Hill-function approximation suggested for T cell exhaustion in (Johnson et al., 2011).

In order to capture effects caused by self (tumor) and non-self (infection) interactions, including significant differences in the magnitude of infection and amount of tumor antigens, we implement the following relationships to mathematically implement the self- / non-self specificity,

$$\alpha_{\rm T} \,<\, \alpha_{\rm I}, \tag{SI-2.4a}$$

$$\kappa_{\rm T} \,>\, \kappa_{\rm I}. \tag{SI-2.4b}$$

Here, subscript labels "T" and "I" correspond to tumor and infection, respectively.

Based on our immunobiochemical reconstruction and following (Warmflash and Dinner, 2009), we make explicitly additional choices to rank TCR-mediated activation parameters as follows,

$$A_c \,\leq\, A_p \,\leq\, A_i \,\leq\, A_b, \tag{SI-2.5a}$$

$$a_c \,\leq\, a_p \,\leq\, a_i \,\leq\, a_b. \tag{SI-2.5b}$$

Based on the developed immunobiochemical reconstruction, the inequality choices (SI-2.5a) ensure that the genes encoding Bcl-6 and PD-1 are activated at lower antigen levels than the genes encoding IRF4 and Blimp-1, whereas the latter ensures that the switch towards the suppression of PD-1 transcription is biased towards the CD8+ T cell, when both IRF4 and Blimp-1 are expressed at high antigen levels.

To account for the abundance of the lumped TNFα/IFNγ species, we have replaced the rate constant σ_p in the equation (SI-2.1b) by the reaction rate expression,

$$\tilde{\sigma}_p \,=\, \sigma_p \,+\, \frac{k_{\rm T} T^{n_T}}{K_T^{n_T} \,+\, T^{n_T}}. \tag{SI-2.6}$$

Here, T corresponds to TNFα, $k_T \,=\, 0.5$, $k_T \,=\, 1$, and $n_T \,=\, 2$. The values of the new parameters are selected in the range of the corresponding parameter values from Table SI-2.1.

SI-2.2 The model parameters

Reference parameter values used in our modeling studies are listed in Table SI-2.1. We have to mention explicitly that the parameter values have not been fitted to any data from (Kohlhapp et al., 2016), and have been selected as follows.

Table SI-2.1. PD-1 expression model parameter values.

Parameters	Values	Comments
σ_i	0.30	IRF4 constituent synthesis rate
σ_p	0.10	PD-1 immune central tolerance const. synth. rate
$a_c = a_p < a_i < a_b$	$0.75 = 0.75 < 75.0 < 100.00$	genetic switch thresholds
$A_c < A_p < A_i < A_b$	$0.01 < 0.10 < 1.00 < 10.00$	genetic switch thresholds
$n_c = n_p$	3	species: Bcl-6 and PD-1
$n_b = n_i$	2	species: Blimp-1 and IRF4
k_b	$0 - 25$	species: IRF4
$k_i = q_i$	7.50	species: Blimp-1 and IRF4
$K_b = K_i = Q_i$	1.00	species: Blimp-1 and IRF4
$m_b = m_i = s_i$	2	species: Blimp-1 and IRF4
$M_b = M_c = M_p$	10.00	species: Blimp-1, Bcl-6 and PD-1
$H_p = H_L$	0.1	species: PD-1 and PD-L1
$r_b = r_c$	2	species: Blimp-1 and Bcl-6
$r_p = h_L$	4	species: PD-1 (p) and PD-L1 (L)
$\mu_c = \mu_p$	0.10	species: Bcl-6 and PD-1
$\mu_b = \mu_i$	1.00	species: Blimp-1 and IRF4
L	0 - 1	species: fraction of PD-1 bound to PD-L1

First, we used dimensionless (scaled) parameter values of the same order of magnitude for the corresponding subsets of parameters as those which were used in (Sciammas et al., 2011; Martinez et al., 2012; Lever et al., 2016).

In our selection of the reference parameter values (Table SI-2.1), we also analyzed and followed a number of insightful discussions of a very challenging and complex problem of selecting relevant parameter values for biological and especially immunological models, presented in a number of published works (Heinrich and Rapoport, 2005; Warmflash and Dinner, 2009; Martinez et al., 2012; Lever et al., 2014; Galvez et al., 2016), including conceptual views (Gunawardena, 2014; Eftimie et al., 2016) as well as discussed general issues with experimental measurements (De Boer and Perelson, 2013; Eftimie et al., 2016).

Second, the parameter values used from (Sciammas et al., 2011; Lever et al., 2016) can be justified for our modeling studies by employing the following IFFL function argument. Indeed, the incoherent feedforward loops cannot exert their biphasic function with any arbitrary parameter values (Kim et al., 2008). The parameter values taken from (Sciammas et al., 2011; Lever et al., 2016) and used in the model (SI-2.1) correspond to the dose-dependent biphasic behaviors as defined and studied in (Kim et al., 2008), and also observed experimentally in the cited literature. In other words, the used parameter values are sufficient to instill the IFFL function.

Finally, the type of modeling carried out in our work can be characterized as phenotypic modeling (Warmflash and Dinner, 2009; Lever et al., 2014; Gunawardena, 2014). Recall that the objective of the phenotypic modeling is to capture the function of a biological system, based on the available and well-established features of the regulatory network under study as also explicitly stated in (Sciammas et al., 2011) which justified the selection of generic Hill functions in their model tailored to the GRN topology. In this work, we implemented a similar approach.

SI-3 THE KPL-IFFL MODEL

For the sake of consistency in the integration of the model (Lever et al., 2016) with our model describing the core circuit, we briefly derive functional relationships needed for the models' integration, adapting the discussion in (Lever et al., 2016).

Specifically, our objective here will be to derive the function $u(\alpha, \kappa)$, which we define as a non-dimensionalized input P in (SI-3.10b), and for which the final expression is given in (SI-3.11). The scaled function $u(\alpha, \kappa)$ depends on two state variables α and κ, the scaled level of Ag and the scaled value of the off-rate constant k_{off}, respectively.

A mathematical model (Lever et al., 2016) is

$$\frac{dL}{dt} = -k_{\text{on}} LR + k_{\text{off}} C_{\text{T}}, \tag{SI-3.1a}$$

$$\frac{dR}{dt} = -k_{\text{on}} LR + k_{\text{off}} C_{\text{T}}, \tag{SI-3.1b}$$

$$\frac{dC_0}{dt} = k_{\text{on}} LR - (k_{\text{off}} + k_{\text{p}})\, C_0, \tag{SI-3.1c}$$

$$\frac{dC_1}{dt} = k_{\text{p}} C_0 - (k_{\text{off}} + k_{\text{i}})\, C_1, \tag{SI-3.1d}$$

$$\frac{dC_2}{dt} = k_{\text{i}} C_1 - k_{\text{off}} C_2, \tag{SI-3.1e}$$

$$\frac{dY}{dt} = \gamma_+^y \left(Y_{\text{T}} - Y\right) - \gamma_-^y Y + \lambda C_1 \left(Y_{\text{T}} - Y\right), \tag{SI-3.1f}$$

$$\frac{dP}{dt} = \gamma_+^p \left(P_{\text{T}} - P\right) - \gamma_-^p P + \delta Y \left(P_{\text{T}} - P\right) - \mu C_1 P. \tag{SI-3.1g}$$

The state variables and parameters of the model (SI-3.1) are defined in (Lever et al., 2016). Parameters important for our derivation are: k_{on} and k_{off} are on- and off-rate constants, k_{p} is the kinetic proofreading rate constant, k_{i} is the kinetic rate constant for transforming of the active complex C_1 into the inactive complex C_2. We will also need C_{T}, the total number of all ligand-receptor complexes,

$$C_{\text{T}} = C_0 + C_1 + C_2. \tag{SI-3.2}$$

Here, C_{T} does not correspond to any conserved moiety and, instead, changes in time.

The model (SI-3.1) has the following first integrals, also termed moiety conservation relationships,

$$L_{\text{T}} = L + C_{\text{T}}. \tag{SI-3.3a}$$

$$R_{\text{T}} = R + C_{\text{T}}, \tag{SI-3.3b}$$

Due to the relationships (SI-3.3b) and (SI-3.3a), the corresponding first two equations (SI-3.1a) and (SI-3.1b) in the model (SI-3.1) become redundant and are omitted from further analysis.

Setting the model linearly independent equations (SI-3.1c) - (SI-3.1g) at steady state, we can obtain the following algebraic relationships,

$$C_0 = \left(\frac{k_{\text{on}}}{k_{\text{off}} + k_{\text{p}}}\right) \times LR, \tag{SI-3.4a}$$

$$C_1 = \left(\frac{k_{\text{p}}}{k_{\text{off}} + k_{\text{i}}}\right) \times C_0, \tag{SI-3.4b}$$

$$C_2 = \left(\frac{k_{\text{i}}}{k_{\text{off}}}\right) \times C_1, \tag{SI-3.4c}$$

$$Y = \left(\frac{1 + \left(\lambda/\gamma_+^y\right) C_1}{1 + \left(\gamma_-^y/\gamma_+^y\right) + \left(\lambda/\gamma_+^y\right) C_1}\right) \times Y_{\text{T}}, \tag{SI-3.4d}$$

$$P = \left(\frac{1 + \left(\delta/\gamma_+^p\right) Y}{1 + \left(\gamma_-^p/\gamma_+^p\right) + \left(\mu/\gamma_+^p\right) C_1 + \left(\delta/\gamma_+^p\right) Y}\right) \times P_{\text{T}}. \tag{SI-3.4e}$$

Next, we eliminate the product LR from (SI-3.4a) by using (SI-3.4a) - (SI-3.4c) in (SI-3.2),

$$C_{\text{T}} = \left(\left(\frac{k_{\text{on}}}{k_{\text{off}} + k_{\text{p}}}\right) + \left(\frac{k_{\text{p}}}{k_{\text{off}} + k_{\text{i}}}\right)\left(\frac{k_{\text{on}}}{k_{\text{off}} + k_{\text{p}}}\right) + \left(\frac{k_{\text{i}}}{k_{\text{off}}}\right)\left(\frac{k_{\text{p}}}{k_{\text{off}} + k_{\text{i}}}\right)\left(\frac{k_{\text{on}}}{k_{\text{off}} + k_{\text{p}}}\right)\right) LR. \tag{SI-3.5}$$

After simple algebraic manipulations, we obtain from (SI-3.5) that

$$LR = K_d C_{\text{T}}, \quad K_d = \frac{k_{\text{off}}}{k_{\text{on}}}. \tag{SI-3.6}$$

Using (SI-3.6) in (SI-3.4a), and then (SI-3.4a) in (SI-3.4b), followed by using (SI-3.4b) in (SI-3.4c), we obtain

$$C_0 = \left(\frac{k_{\text{off}}}{k_{\text{off}} + k_{\text{p}}}\right) C_{\text{T}}, \tag{SI-3.7a}$$

$$C_1 = \left(\frac{k_{\text{p}}}{k_{\text{off}} + k_{\text{i}}}\right)\left(\frac{k_{\text{off}}}{k_{\text{off}} + k_{\text{p}}}\right) C_{\text{T}}, \tag{SI-3.7b}$$

$$C_2 = \left(\frac{k_{\text{i}}}{k_{\text{off}}}\right)\left(\frac{k_{\text{p}}}{k_{\text{off}} + k_{\text{i}}}\right)\left(\frac{k_{\text{off}}}{k_{\text{off}} + k_{\text{p}}}\right) C_{\text{T}}. \tag{SI-3.7c}$$

Note that C_{T} is still unknown in (SI-3.7). To compute C_{T}, we use an alternative expression for the product LR.

Indeed, we can obtain from (SI-3.3a) and (SI-3.3b) that $L = L_{\text{T}} - C_{\text{T}}$ and $R = R_{\text{T}} - C_{\text{T}}$, respectively. Now, using $LR = (L_{\text{T}} - C_{\text{T}})(R_{\text{T}} - C_{\text{T}})$ in (SI-3.6), we come to a closed quadratic equation with respect to C_{T},

$$(L_{\text{T}} - C_{\text{T}})(R_{\text{T}} - C_{\text{T}}) = K_d C_{\text{T}}. \tag{SI-3.8}$$

Solving the quadratic equation (SI-3.8) with respect to C_{T}, we obtain two solutions, only one of which corresponds to the biologically meaningful condition, $C_{\mathrm{T}} = 0$ at $L_{\mathrm{T}} = 0$,

$$C_{\mathrm{T}} = \frac{1}{2}\left(R_{\mathrm{T}} + L_{\mathrm{T}} + K_d - \sqrt{\left(R_{\mathrm{T}} + L_{\mathrm{T}} + K_d\right)^2 - 4R_{\mathrm{T}}L_{\mathrm{T}}}\right). \tag{SI-3.9}$$

The solution (SI-3.9) also corresponds to the stable equilibrium in the system of linearly independent equations (SI-3.1c) - (SI-3.1g).

It is convenient to nondimensionalize the equilibrium solution of (SI-3.1) given by the expressions (SI-3.4a) - (SI-3.4e), and (SI-3.9) by scaling all state variables and parameters as follows,

$$c_{\mathrm{T}} = \frac{C_{\mathrm{T}}}{R_{\mathrm{T}}}, \quad c_k = \frac{C_k}{R_{\mathrm{T}}}, \quad k = 0, 1, 2, \tag{SI-3.10a}$$

$$y = \frac{Y}{Y_{\mathrm{T}}}, \quad u = \frac{P}{P_{\mathrm{T}}}, \tag{SI-3.10b}$$

$$K_{\mathrm{p}} = \frac{1}{R_{\mathrm{T}}}\left(\frac{k_{\mathrm{p}}}{k_{\mathrm{on}}}\right), \quad K_{\mathrm{i}} = \frac{1}{R_{\mathrm{T}}}\left(\frac{k_{\mathrm{i}}}{k_{\mathrm{on}}}\right), \tag{SI-3.10c}$$

$$\Gamma^y = \frac{\gamma_-^y}{\gamma_+^y}, \quad \Gamma^p = \frac{\gamma_-^p}{\gamma_+^p}, \tag{SI-3.10d}$$

$$\Lambda = \lambda\frac{R_{\mathrm{T}}}{\gamma_+^y}, \quad \Delta = \delta\frac{Y_{\mathrm{T}}}{\gamma_+^p}, \quad \Theta = \mu\frac{R_{\mathrm{T}}}{\gamma_+^p}, \tag{SI-3.10e}$$

$$\alpha = \frac{L_{\mathrm{T}}}{R_{\mathrm{T}}}, \quad \kappa = \frac{K_d}{R_{\mathrm{T}}}. \tag{SI-3.10f}$$

We obtain from the rescaled (SI-3.4e) that

$$u(\alpha, \kappa) = \frac{1 + \Delta\, y(\alpha, \kappa)}{1 + \Gamma^p + \Theta v(\kappa)\, c_{\mathrm{T}}(\alpha, \kappa) + \Delta\, y(\alpha, \kappa)}. \tag{SI-3.11}$$

In (SI-3.11), the functions $c_1(\alpha)$ and $y(\alpha)$ are obtained from the corresponding expressions (SI-3.4b) and (SI-3.4d) rescaled as discussed earlier,

$$y(\alpha, \kappa) = \frac{1 + \Lambda v(\kappa)\, c_{\mathrm{T}}(\alpha, \kappa)}{1 + \Gamma^y + \Lambda v(\kappa)\, c_{\mathrm{T}}(\alpha, \kappa)}, \tag{SI-3.12a}$$

$$c_{\mathrm{T}}(\alpha, \kappa) = \frac{1}{2}\left(1 + \alpha + \kappa - \sqrt{(1 + \alpha + \kappa)^2 - 4\alpha}\right), \tag{SI-3.12b}$$

$$v(\kappa) = \left(\frac{K_{\mathrm{p}}}{\kappa + K_{\mathrm{i}}}\right)\left(\frac{\kappa}{\kappa + K_{\mathrm{p}}}\right). \tag{SI-3.12c}$$

Reference values of parameters used in the expressions (SI-3.11) - (SI-3.12) are listed in Table SI-3.1. These values correspond to the values used to compute Fig. 3 in (Lever et al., 2016).

Table SI-3.1. KPL-IFFL model parameter values.

№	Parameter	Value
1.	K_i	10^{-3}
2.	K_p	10^{-2}
3.	Γ^y	5×10^2
4.	Γ^p	5×10^2
5.	Δ	5×10^3
6.	Θ	5×10^4
7.	Λ	10^4
8.	α	$10^{-4} - 10^4$
9.	κ	$10^{-4} - 10^2$

SI-4 ANALYSIS OF SPARSE VERSUS DENSE EXPERIMENTAL DATA

The main limitation of experimental data (Kohlhapp et al., 2016) is that the data is sparse. Yet, in spite of this limitation, by focusing on the phenotypes (A) and (B) schematically depicted in Fig. 8, our model semi-quantitatively fits a body of experimental data both discussed in the current literature and in (Kohlhapp et al., 2016) with very a small number of variables and parameters.

The topic of limitations imposed by the sparsity of experimental data has been widely discussed in the biological and especially immunological literature in the context of the applicability of such data in mathematical modeling (De Boer and Perelson, 2013; François et al., 2013; Gunawardena, 2014; Eftimie et al., 2016) to mention just a few references.

Small-scale models are highly interpretative (James et al., 2013; Ledzewicz and Schattler, 2017) and, here, we agree with the following citation: "Simplified models are sometimes more predictive than elaborate ones when data are sparse and have the added benefit of transparency" (François et al., 2013). An added benefit of smaller and more phenomenological models is that they have a small number of parameters, for which one may be able to find rough estimates from the literature. In contrast, large scale models have many parameters, most of which may not be available from the literature and, instead, should be fitted to data. Such models may be more powerful in accurate predictions at the (possible) expense of loosing interpretability (James et al., 2013).

SI-5 MATHEMATICAL AND NUMERICAL METHODS

The steady-state solutions of the models developed in this work, the solution stability (Sontag, 2013), as well as the parameter continuation of the steady-state solutions (Kuznetsov, 2013) have been studied numerically (Khibnik et al., 1993), using the command-line functionality of `matcont6p10`, a Matlab®-based Continuation Toolbox (Dhooge et al., 2008). MATLAB® Parallel Computing Toolbox was employed whenever possible. Finally, the color maps were generated using `varycolor.m`, a Matlab®-based function.

REFERENCES

Aleksic, M., Dushek, O., Zhang, H., Shenderov, E., Chen, J. L., Cerundolo, V., et al. (2010). Dependence of T cell antigen recognition on T cell receptor-peptide MHC confinement time. *Immunity* 32, 163–174

Altan-Bonnet, G. and Germain, R. N. (2005). Modeling T cell antigen discrimination based on feedback control of digital ERK responses. *PLoS Biol.* 3, e356

Baaten, B. J., Cooper, A. M., Swain, S. L., and Bradley, L. M. (2013). Location, location, location: the impact of migratory heterogeneity on T cell function. *Frontiers in immunology* 4

Bardhan, K., Anagnostou, T., and Boussiotis, V. A. (2016). The PD1:PD-L1/2 pathway from discovery to clinical implementation. *Front Immunol* 7, 550

Beattie, L., Peltan, A., Maroof, A., Kirby, A., Brown, N., Coles, M., et al. (2010). Dynamic imaging of experimental Leishmania donovani-induced hepatic granulomas detects Kupffer cell-restricted antigen presentation to antigen-specific CD8+ T cells. *PLoS pathogens* 6, e1000805

Beider, K., Nagler, A., Wald, O., Franitza, S., Dagan-Berger, M., Wald, H., et al. (2003). Involvement of CXCR4 and IL-2 in the homing and retention of human NK and NK T cells to the bone marrow and spleen of NOD/SCID mice. *Blood* 102, 1951–1958

Bhat, P., Leggatt, G., Matthaei, K. I., and Frazer, I. H. (2014). The kinematics of cytotoxic lymphocytes influence their ability to kill target cells. *PLoS ONE* 9, e95248

Biotec, M. and Gladbach, B. (2011). In vivo imaging of T-cell motility in the elicitation phase of contact hypersensitivity using two-photon microscopy. *J Investig Dermatol* 131, 977–979

Boissonnas, A., Fetler, L., Zeelenberg, I. S., Hugues, S., and Amigorena, S. (2007). In vivo imaging of cytotoxic T cell infiltration and elimination of a solid tumor. *Journal of Experimental Medicine* 204, 345–356

Breart, B., Lemaître, F., Celli, S., and Bousso, P. (2008). Two-photon imaging of intratumoral CD8+ T cell cytotoxic activity during adoptive T cell therapy in mice. *The Journal of clinical investigation* 118, 1390

Brown, K. E., Freeman, G. J., Wherry, E. J., and Sharpe, A. H. (2010). Role of PD-1 in regulating acute infections. *Curr. Opin. Immunol.* 22, 397–401

Calzascia, T., Masson, F., Di Berardino-Besson, W., Contassot, E., Wilmotte, R., Aurrand-Lions, M., et al. (2005). Homing phenotypes of tumor-specific CD8 T cells are predetermined at the tumor site by crosspresenting APCs. *Immunity* 22, 175–184

Celli, S., Albert, M. L., and Bousso, P. (2011). Visualizing the innate and adaptive immune responses underlying allograft rejection by two-photon microscopy. *Nature medicine* 17, 744–749

Chimen, M., Apta, B. H., and Mcgettrick, H. M. (2017). Introduction: T cell trafficking in inflammation and immunity. In *T-Cell Trafficking* (Springer). 73–84

Coombs, D., Dushek, O., and van der Merwe, P. A. (2011). A review of mathematical models for T cell receptor triggering and antigen discrimination. In *Mathematical Models and Immune Cell Biology* (Springer). 25–45

Courtney, A. H., Lo, W. L., and Weiss, A. (2017). TCR signaling: mechanisms of initiation and propagation. *Trends Biochem. Sci.*

Das, D. K., Feng, Y., Mallis, R. J., Li, X., Keskin, D. B., Hussey, R. E., et al. (2015). Force-dependent transition in the T-cell receptor β-subunit allosterically regulates peptide discrimination and pMHC bond lifetime. *Proc. Natl. Acad. Sci. U.S.A.* 112, 1517–1522

De Boer, R. J. and Perelson, A. S. (2013). Quantifying T lymphocyte turnover. *J. Theor. Biol.* 327, 45–87

de Oliveira, K. B., Guembarovski, R. L., Guembarovski, A. M. F. L., do Amaral, A. C. d. S., Sobrinho, W. J., Ariza, C. B., et al. (2013). CXCL12, CXCR4 and IFNγ genes expression: implications for proinflammatory microenvironment of breast cancer. *Clinical and Experimental Medicine* 13, 211–219

Deguine, J., Breart, B., Lemaître, F., Di Santo, J. P., and Bousso, P. (2010). Intravital imaging reveals distinct dynamics for natural killer and CD8+ T cells during tumor regression. *Immunity* 33, 632–644

Dhooge, A., Govaerts, W., Kuznetsov, Y. A., Meijer, H. G. E., and Sautois, B. (2008). New features of the software matcont for bifurcation analysis of dynamical systems. *Mathematical and Computer Modelling of Dynamical Systems* 14, 147–175

Donnadieu, E. (2016). *Defects in T Cell Trafficking and Resistance to Cancer Immunotherapy* (Springer)

Dufour, J. H., Dziejman, M., Liu, M. T., Leung, J. H., Lane, T. E., and Luster, A. D. (2002). IFN-gamma-inducible protein 10 (IP-10; CXCL10)-deficient mice reveal a role for IP-10 in effector T cell generation and trafficking. *J. Immunol.* 168, 3195–3204

Eftimie, R., Gillard, J. J., and Cantrell, D. A. (2016). Mathematical models for immunology: current state of the art and future research directions. *Bull. Math. Biol.* 78, 2091–2134

Escors, D., Bricogne, C., Arce, F., Kochan, G., and Karwacz, K. (2011). On the Mechanism of T cell receptor down-modulation and its physiological significance. *J Biosci Med* 1

Feinerman, O., Germain, R. N., and Altan-Bonnet, G. (2008). Quantitative challenges in understanding ligand discrimination by $\alpha\beta$ T cells. *Mol. Immunol.* 45, 619–631

Fife, B. T., Pauken, K. E., Eagar, T. N., Obu, T., Wu, J., Tang, Q., et al. (2009). Interactions between PD-1 and PD-L1 promote tolerance by blocking the TCR-induced stop signal. *Nat. Immunol.* 10, 1185–1192

Francisco, L. M., Sage, P. T., and Sharpe, A. H. (2010). The PD-1 pathway in tolerance and autoimmunity. *Immunol. Rev.* 236, 219–242

François, P. and Altan-Bonnet, G. (2016). The case for absolute ligand discrimination: modeling information processing and decision by immune T cells. *Journal of Statistical Physics* 162, 1130–1152

François, P., Voisinne, G., Siggia, E. D., Altan-Bonnet, G., and Vergassola, M. (2013). Phenotypic model for early T-cell activation displaying sensitivity, specificity, and antagonism. *Proc. Natl. Acad. Sci. U.S.A.* 110, E888–897

Freeman, G. J., Long, A. J., Iwai, Y., Bourque, K., Chernova, T., Nishimura, H., et al. (2000). Engagement of the PD-1 immunoinhibitory receptor by a novel B7 family member leads to negative regulation of lymphocyte activation. *J. Exp. Med.* 192, 1027–1034

Galvez, J., Galvez, J. J., and Garcia-Penarrubia, P. (2016). TCR/pMHC interaction: phenotypic model for an unsolved enigma. *Front Immunol* 7, 467

Garcia, Z., Pradelli, E., Celli, S., Beuneu, H., Simon, A., and Bousso, P. (2007). Competition for antigen determines the stability of T cell-dendritic cell interactions during clonal expansion. *Proc. Natl. Acad. Sci. U.S.A.* 104, 4553–4558

Grakoui, A., Bromley, S. K., Sumen, C., Davis, M. M., Shaw, A. S., Allen, P. M., et al. (1999). The immunological synapse: a molecular machine controlling T cell activation. *Science* 285, 221–227

Grossman, Z. and Paul, W. E. (1992). Adaptive cellular interactions in the immune system: the tunable activation threshold and the significance of subthreshold responses. *Proc. Natl. Acad. Sci. U.S.A.* 89, 10365–10369

Grossman, Z. and Paul, W. E. (2001). Autoreactivity, dynamic tuning and selectivity. *Curr. Opin. Immunol.* 13, 687–698

Grossman, Z. and Paul, W. E. (2015). Dynamic tuning of lymphocytes: physiological basis, mechanisms, and function. *Annu. Rev. Immunol.* 33, 677–713

Gunawardena, J. (2014). Models in biology: 'accurate descriptions of our pathetic thinking'. *BMC biology* 12, 29

Heinrich, R. and Rapoport, T. A. (2005). Generation of nonidentical compartments in vesicular transport systems. *J. Cell Biol.* 168, 271–280

Hogquist, K. A. and Jameson, S. C. (2014). The self-obsession of T cells: how TCR signaling thresholds affect fate 'decisions' and effector function. *Nat. Immunol.* 15, 815–823

Honda, T., Egen, J. G., Lammermann, T., Kastenmuller, W., Torabi-Parizi, P., and Germain, R. N. (2014). Tuning of antigen sensitivity by T cell receptor-dependent negative feedback controls T cell effector function in inflamed tissues. *Immunity* 40, 235–247

Hopfield, J. J. (1974). Kinetic proofreading: a new mechanism for reducing errors in biosynthetic processes requiring high specificity. *Proc. Natl. Acad. Sci. U.S.A.* 71, 4135–4139

Irving, M., Zoete, V., Hebeisen, M., Schmid, D., Baumgartner, P., Guillaume, P., et al. (2012). Interplay between T cell receptor binding kinetics and the level of cognate peptide presented by major histocompatibility complexes governs CD8+ T cell responsiveness. *J. Biol. Chem.* 287, 23068–23078

James, G., Witten, D., Hastie, T., and Tibshirani, R. (2013). *An Introduction to Statistical Learning*, vol. 112 (Springer)

Jennrich, S., Lee, M. H., Lynn, R. C., Dewberry, K., and Debes, G. F. (2012). Tissue exit: a novel control point in the accumulation of antigen-specific CD8 T cells in the influenza a virus-infected lung. *J. Virol.* 86, 3436–3445

Johnson, P. L., Kochin, B. F., McAfee, M. S., Stromnes, I. M., Regoes, R. R., Ahmed, R., et al. (2011). Vaccination alters the balance between protective immunity, exhaustion, escape, and death in chronic infections. *J. Virol.* 85, 5565–5570

Joyce, J. A. and Fearon, D. T. (2015). T cell exclusion, immune privilege, and the tumor microenvironment. *Science* 348, 74–80

Karwacz, K., Arce, F., Bricogne, C., Kochan, G., and Escors, D. (2012). PD-L1 co-stimulation, ligand-induced TCR down-modulation and anti-tumor immunotherapy. *Oncoimmunology* 1, 86–88

Karwacz, K., Bricogne, C., MacDonald, D., Arce, F., Bennett, C. L., Collins, M., et al. (2011). PD-L1 co-stimulation contributes to ligand-induced T cell receptor down-modulation on CD8+ T cells. *EMBO Mol Med* 3, 581–592

Khibnik, A. I., Kuznetsov, Y. A., Levitin, V. V., and Nikolaev, E. V. (1993). Continuation techniques and interactive software for bifurcation analysis of ODEs and iterated maps. *Physica D: Nonlinear Phenomena* 62, 360–371

Kim, D., Kwon, Y. K., and Cho, K. H. (2008). The biphasic behavior of incoherent feed-forward loops in biomolecular regulatory networks. *Bioessays* 30, 1204–1211

Kim, J. M. and Chen, D. S. (2016). Immune escape to PD-L1/PD-1 blockade: seven steps to success (or failure). *Ann. Oncol.*

Kindt, T. J., Goldsby, R. A., Osborne, B. A., and Kuby, J. (2007). *Kuby Immunology* (W.H.Freeman and Company, New York)

Kohlhapp, F. J., Huelsmann, E. J., Lacek, A. T., Schenkel, J. M., Lusciks, J., Broucek, J. R., et al. (2016). Non-oncogenic Acute Viral Infections Disrupt Anti-cancer Responses and Lead to Accelerated Cancer-Specific Host Death. *Cell Rep* 17, 957–965

Kosinsky, Y., Dovedi, S. J., Peskov, K., Voronova, V., Chu, L., Tomkinson, H., et al. (2018). Radiation and PD-(L)1 treatment combinations: immune response and dose optimization via a predictive systems model. *J Immunother Cancer* 6, 17

Kuznetsov, Y. A. (2013). *Elements of Applied Bifurcation Theory*, vol. 112 (Springer Science & Business Media)

Ledzewicz, U. and Schattler, H. (2017). Application of mathematical models to metronomic chemotherapy: What can be inferred from minimal parameterized models? *Cancer Lett.* 401, 74–80

Lever, M., Lim, H. S., Kruger, P., Nguyen, J., Trendel, N., Abu-Shah, E., et al. (2016). Architecture of a minimal signaling pathway explains the T-cell response to a 1 million-fold variation in antigen affinity and dose. *Proc. Natl. Acad. Sci. U.S.A.* 113, E6630–E6638

Lever, M., Maini, P. K., van der Merwe, P. A., and Dushek, O. (2014). Phenotypic models of T cell activation. *Nat. Rev. Immunol.* 14, 619–629

Levin, D., Forrest, S., Banerjee, S., Clay, C., Cannon, J., Moses, M., et al. (2016). A spatial model of the efficiency of T cell search in the influenza-infected lung. *J. Theor. Biol.* 398, 52–63

Liechtenstein, T., Dufait, I., Bricogne, C., Lanna, A., Pen, J., Breckpot, K., et al. (2012). PD-L1/PD-1 co-stimulation, a brake for T cell activation and a T cell differentiation signal. *J Clin Cell Immunol* S12

Liu, B., Chen, W., Evavold, B. D., and Zhu, C. (2014). Accumulation of dynamic catch bonds between TCR and agonist peptide-MHC triggers T cell signaling. *Cell* 157, 357–368

Marchuk, G. I. (1997). *Mathematical Modelling of Immune Response in Infectious Diseases*, vol. 395 (Springer Science & Business Media)

Marelli-Berg, F. M., Fu, H., Vianello, F., Tokoyoda, K., and Hamann, A. (2010). Memory T-cell trafficking: new directions for busy commuters. *Immunology* 130, 158–165

Martinez, M. R., Corradin, A., Klein, U., Alvarez, M. J., Toffolo, G. M., di Camillo, B., et al. (2012). Quantitative modeling of the terminal differentiation of B cells and mechanisms of lymphomagenesis. *Proc. Natl. Acad. Sci. U.S.A.* 109, 2672–2677

McKeithan, T. W. (1995). Kinetic proofreading in T-cell receptor signal transduction. *Proc. Natl. Acad. Sci. U.S.A.* 92, 5042–5046

Nirschl, C. J. and Drake, C. G. (2013). Molecular pathways: coexpression of immune checkpoint molecules: signaling pathways and implications for cancer immunotherapy. *Clin. Cancer Res.* 19, 4917–4924

Oelkrug, C. and Ramage, J. M. (2014). Enhancement of T cell recruitment and infiltration into tumours. *Clin. Exp. Immunol.* 178, 1–8

Ogawa, N., Ping, L., Zhenjun, L., Takada, Y., and Sugai, S. (2002). Involvement of the interferon-γ–induced T cell–attracting chemokines, interferon-γ–inducible 10-kd protein (CXCL10) and monokine induced by interferon-γ (CXCL9), in the salivary gland lesions of patients with Sjögren's syndrome. *Arthritis & Rheumatism* 46, 2730–2741

Ortega-Carrion, A. and Vicente-Manzanares, M. (2016). Concerning immune synapses: a spatiotemporal timeline. *F1000Research* 5

Parello, C. S. and Huseby, E. S. (2015). Indoctrinating T cells to attack pathogens through homeschooling. *Trends Immunol.* 36, 337–343

Pauken, K. E., Sammons, M. A., Odorizzi, P. M., Manne, S., Godec, J., Khan, O., et al. (2016). Epigenetic stability of exhausted T cells limits durability of reinvigoration by PD-1 blockade. *Science* 354, 1160–1165

Pauken, K. E. and Wherry, E. J. (2015a). Overcoming T cell exhaustion in infection and cancer. *Trends Immunol.* 36, 265–276

Pauken, K. E. and Wherry, E. J. (2015b). Snapshot: T cell exhaustion. *Cell* 163, 1038–1038

Poleszczuk, J. T., Luddy, K. A., Prokopiou, S., Robertson-Tessi, M., Moros, E. G., Fishman, M., et al. (2016). Abscopal Benefits of Localized Radiotherapy Depend on Activated T-cell Trafficking and Distribution between Metastatic Lesions. *Cancer Res.* 76, 1009–1018

Rendall, A. D. and Sontag, E. D. (2017). Multiple steady states and the form of response functions to antigen in a model for the initiation of T-cell activation. *R Soc Open Sci* 4, 170821

Richards, D. M., Kyewski, B., and Feuerer, M. (2016). Re-examining the nature and function of self-reactive T cells. *Trends Immunol.* 37, 114–125

Sakaguchi, S., Yamaguchi, T., Nomura, T., and Ono, M. (2008). Regulatory T cells and immune tolerance. *Cell* 133, 775–787

Schietinger, A. and Greenberg, P. D. (2014). Tolerance and exhaustion: defining mechanisms of T cell dysfunction. *Trends Immunol.* 35, 51–60

Sciammas, R., Li, Y., Warmflash, A., Song, Y., Dinner, A. R., and Singh, H. (2011). An incoherent regulatory network architecture that orchestrates B cell diversification in response to antigen signaling. *Mol. Syst. Biol.* 7, 495

Sharpe, A. H. and Pauken, K. E. (2017). The diverse functions of the PD1 inhibitory pathway. *Nat. Rev. Immunol.*

Simon, S. and Labarriere, N. (2017). PD-1 expression on tumor-specific T cells: Friend or foe for immunotherapy? *OncoImmunology* 0, 1–7

Sontag, E. D. (2013). *Mathematical Control Theory: Deterministic Finite Dimensional Systems*, vol. 6 (Springer)

Speiser, D. E., Ho, P. C., and Verdeil, G. (2016). Regulatory circuits of T cell function in cancer. *Nat. Rev. Immunol.* 16, 599–611

Spranger, S. (2016). Mechanisms of tumor escape in the context of the T-cell-inflamed and the non-T-cell-inflamed tumor microenvironment. *Int. Immunol.* 28, 383–391

Stein, J. V., Moalli, F., and Ackerknecht, M. (2016). Basic rules of T cell migration. In *Defects in T Cell Trafficking and Resistance to Cancer Immunotherapy* (Springer). 1–19

Tan, M. P., Gerry, A. B., Brewer, J. E., Melchiori, L., Bridgeman, J. S., Bennett, A. D., et al. (2015). T cell receptor binding affinity governs the functional profile of cancer-specific CD8+ T cells. *Clin. Exp. Immunol.* 180, 255–270

Tkach, K. and Altan-Bonnet, G. (2013). T cell responses to antigen: hasty proposals resolved through long engagements. *Curr. Opin. Immunol.* 25, 120–125

Toapanta, F. R. and Ross, T. M. (2009). Impaired immune responses in the lungs of aged mice following influenza infection. *Respir. Res.* 10, 112

Van Braeckel-Budimir, N. and Harty, J. T. (2017). Influenza-induced lung Trm: not all memories last forever. *Immunol. Cell Biol.* 95, 651–655

Vianello, F., Olszak, I. T., and Poznansky, M. C. (2005). Fugetaxis: active movement of leukocytes away from a chemokinetic agent. *J. Mol. Med.* 83, 752–763

Vonderheide, R. H. and June, C. H. (2014). Engineering T cells for cancer: our synthetic future. *Immunol. Rev.* 257, 7–13

Wang, C., Singer, M., and Anderson, A. C. (2017). Molecular dissection of CD8(+) T-cell dysfunction. *Trends Immunol.* 38, 567–576

Warmflash, A. and Dinner, A. R. (2009). Modeling gene regulatory networks for cell fate specification. *Statistical Mechanics of Cellular Systems and Processes* , 121

Wherry, E. J., Ha, S. J., Kaech, S. M., Haining, W. N., Sarkar, S., Kalia, V., et al. (2007). Molecular signature of CD8+ T cell exhaustion during chronic viral infection. *Immunity* 27, 670–684

Xie, J., Tato, C. M., and Davis, M. M. (2013). How the immune system talks to itself: the varied role of synapses. *Immunological reviews* 251, 65–79

Zhang, Y. and Rundell, A. (2006). Comparative study of parameter sensitivity analyses of the TCR-activated Erk-MAPK signalling pathway. *Syst Biol (Stevenage)* 153, 201–211

Zinselmeyer, B. H., Heydari, S., Sacristan, C., Nayak, D., Cammer, M., Herz, J., et al. (2013). PD-1 promotes immune exhaustion by inducing antiviral T cell motility paralysis. *J. Exp. Med.* 210, 757–774